Research Square

Preprints are preliminary reports that have not undergone peer review.
They should not be considered conclusive, used to inform clinical practice,
or referenced by the media as validated information.

Xener: Bidirectional evidence propagation on a plant cell-type knowledge graph for traceable cross-species annotation

Hansheng Zhao

zhaohansheng@icbr.ac.cn

Institute of Gene Science and Industrialization for Bamboo and Rattan Resources, International Centre for Bamboo and Rattan, Beijing 100102, China https://orcid.org/0000-0002-5405-0375

Huan Zhang

International Centre for Bamboo and Rattan

Shuai Liu

BGI Research https://orcid.org/0009-0008-3203-1158

Lei Cao

BGI Research, Beijing

Zeyu Fan

International Centre for Bamboo and Rattan

Shuangsang Fang

BGI Research https://orcid.org/0000-0002-4126-0074

Huanming Yang

BGI-Shenzhen https://orcid.org/0000-0002-0858-3410

Article

Keywords:

Posted Date: November 12th, 2026

DOI: https://doi.org/10.21203/rs.3.rs-11244739/v1

License: This work is licensed under a Creative Commons Attribution 4.0 International License.
Read Full License

Additional Declarations: Yes there is potential Competing Interest. L.C and S.F are named inventors on granted Chinese patent CN121415883B (application No. 202511884187.0), which relates to the cell annotation methodology described in this study. The remaining authors declare no competing interests.

Xener: Bidirectional evidence propagation on a plant cell-type knowledge graph for traceable cross-species annotation

Affiliations

Huan Zhang[1,2†], Shuai Liu[2†], Lei Cao[2†], Zeyu Fan[1,3], Shuangsang Fang[2*], Hansheng Zhao[1*], Huanming Yang[4]

[1] International Centre for Bamboo and Rattan, Beijing 100102, China

[2] BGI Research, Beijing 100083, China

[3] Geneplus-Beijing Institute, Beijing 102206, China

[4] BGI Research, Shenzhen 518083, China

†These authors contributed equally to this work.

Contributions

H. Zhang, L.C., and H. Zhao conceptualized and designed the research. H. Zhang and S.L. developed the methodology and software, curated the data, performed the computational analyses, and prepared the figures. Z.F. contributed to the investigation and validation, and H.Y. provided resources and advised on the study. H. Zhang, S.L., and H. Zhao wrote the original draft. H. Zhao and S.F. supervised the project, acquired funding, and reviewed and edited the manuscript. All the authors read and approved the final manuscript.

Corresponding author

Correspondence to: Shuangsang Fang & Hansheng Zhao

Shuangsang Fang. BGI Research, Beijing 100083, China. Email: fangshuangsang@genomics.cn;

Hansheng Zhao. International Centre for Bamboo and Rattan, Beijing 100102, China. Email: zhaohansheng@icbr.ac.cn.

ORCIDs

Huan Zhang (0009-0007-6974-3864); Shuai Liu (0009-0008-3203-1158); Lei Cao (0000-0002-7170-9602); Zeyu Fan (0000-0002-2792-0902); Huanming Yang (0000-0002-0858-3410); Hansheng Zhao (0000-0002-5405-0375); Shuangsang Fang (0000-0002-4126-0074)

Abstract

The cross-species annotation of plant single-cell data is limited by sparse reference atlases, one-to-many homology relationships, and context-dependent marker specificity, particularly in nonmodel species. We developed Xener, a reference-independent framework integrating a heterogeneous plant cell-type knowledge graph with bidirectional evidence propagation. Xener-Anno propagates evidence from cluster-level differentially expressed genes through protein homology, marker–cell-type associations, and Plant Ontology (PO) relationships to identify the most specific supported identity. Xener-Refine projects identity evidence onto individual cells, resolving within-cluster heterogeneity and recovering minority populations without reclustering. Across 62 datasets from 24 species, Xener achieved the highest hierarchical concordance in 46 datasets and outperformed the reference-independent methods GPTCelltype and PubMed-SKILL in terms of mean and

median concordance. Compared with reference-dependent SATURN, Xener achieved 3.47-fold higher median concordance. In a Brassica rapa atlas, Xener resolved bundle sheath annotations into transcriptionally distinct candidate populations supported by traceable gene–homolog–cell-type paths. We further compiled Xener-Markers, an orthogroup-linked cross-species resource that classifies candidate markers as Core, Broad, Narrow, or Unique across 38 PO cell types. With respect to the spatial data for bamboo, Xener integrated evidence from Arabidopsis thaliana and rice, reaching 87.5% spot-weighted agreement with published labels; RNA in situ hybridization supported the localization of candidate marker clrGene018032. Thus, Xener extends traceable cell-type annotation beyond well-characterized model species.

Introduction

Plant tissues comprise diverse cell types whose identities, developmental states, and responses to the environment are obscured in bulk transcriptomes but can be resolved via single-cell and single-nucleus transcriptomics (Ryu et al., 2021; Seyfferth et al., 2021). Following foundational single-cell studies in Arabidopsis (Denyer et al., 2019; Ryu et al., 2019; Shulse et al., 2019; Shahan et al., 2022), cellular atlases have been generated for additional plant species, including rice (Oryza sativa; Wang et al., 2021), maize (Zea mays; Xu et al., 2021; Marand et al., 2021), wheat (Triticum aestivum; Ke et al., 2025), and bamboo (Phyllostachys edulis; Qin et al., 2025). Spatial transcriptomics further relates molecular states to anatomical position (Yin et al., 2023; Yu et al., 2023). Together, these resources advance efforts toward a broader Plant Cell Atlas, but their

expansion does not by itself make cell-type labels comparable across species (Rhee et al., 2019; Lee et al., 2025). Populations assigned similar labels can differ in marker expression even when related cellular functions are conserved (Guillotin et al., 2023; Chau et al., 2025). Cross-species analysis therefore requires determining which populations correspond, at what level of cellular identity, and on the basis of what evidence (Liu et al., 2023; Zhong et al., 2025). Such correspondence is essential both for annotating species without a suitable reference atlas and for distinguishing conserved cellular programs from lineage-specific cellular ones (Xue et al., 2025; Tarashansky et al., 2021).

This problem is particularly acute in nonmodel plants, for which validated markers and annotated single-cell references remain sparse (Rhaman et al., 2024; Nobori, 2025). Gene homology does not translate directly into cell-type equivalence: one-to-many relationships, whole-genome duplication, and lineage-specific gene-family expansion can generate paralogs that partition ancestral functions or acquire new roles (Panchy et al., 2016; Guillotin et al., 2023; Passalacqua and Gillis, 2024). Marker specificity is likewise context dependent and varies among species, tissues, developmental stages, and physiological states (Tenorio Berrío and Dubois, 2024; Chau et al., 2025). Existing plant marker databases differ in terms of species coverage and cell-type granularity (Chen et al., 2021; Jin et al., 2022; He et al., 2024; Zheng et al., 2026), whereas Plant Ontology (PO) terms are hierarchical, such that available evidence may support a broad parent identity without the resolution of a specific subtype (Cooper et al., 2013; Walls et al., 2012). Robust

cross-species annotation therefore requires reconciling expression, homology, marker provenance, and ontology structure under incomplete and uneven prior knowledge.

Current annotation strategies rely on expert curation or automated label assignment (Cheng et al., 2023; Clarke et al., 2021). Expert curation remains valuable but is time-consuming and dependent on specialist judgment. Reference-dependent workflows assign cell identities by aligning query profiles with labeled populations in an annotated atlas (Aran et al., 2019; Stuart et al., 2019; Kang et al., 2021; Lotfollahi et al., 2022). While within-species transfer operates in a shared gene space, cross-species transfer depends on connecting query and reference genes through orthology, broader homology, or sequence-derived representations. SATURN, for example, uses protein language model embeddings to construct a shared cross-species representation without restricting the mapping to one-to-one orthologs (Rosen et al., 2024). Reference-dependent annotation nevertheless requires suitable labeled populations that correspond biologically to the query, which are often unavailable outside well-characterized model species (Ke et al., 2025). Reference-independent approaches instead compare query-cluster markers with curated marker knowledge (Pliner et al., 2019; Zhang et al., 2019; Shao et al., 2020; Ianevski et al., 2022) or use large language models to infer labels from marker lists, as exemplified by GPTCelltype (Hou and Ji, 2024) and PubMed-SKILL (https://github.com/FFFold/PubMed-SKILL). Orthogroup-based aggregation of markers has likewise been used to determine cell identities across species without the need for cross-species data integration (Chau et al., 2025). However, the typical outputs of these approaches are labels or scores rather than a structured chain linking query genes, homologs,

marker records, ontology terms, and the resulting label. Therefore, the traceability of assignments and the reuse of annotation evidence for resolving heterogeneous clusters are limited.

Here, we developed Xener, a reference-independent, knowledge-guided framework for cross-species plant cell-type annotation. Xener integrates a heterogeneous plant cell-type knowledge graph (KG) with bidirectional evidence propagation. Xener-Anno propagates evidence from query-cluster differentially expressed genes (DEGs) through protein homology, marker–cell-type, and PO relationships, and uses ontology-aware backtracking to report the most specific identity supported by the available evidence. Xener-Refine reverses this flow by projecting identity-specific evidence onto individual cells, enabling evidence-supported resolution of within-cluster heterogeneity while retaining the paths underlying each assignment. We evaluated Xener across 62 datasets from 24 plant species, integrated standardized marker evidence from Xener-annotated datasets using cross-species gene homology to construct the Xener-Markers resource, and applied the framework to cross-species single-cell and bamboo spatial transcriptomic data. By converting fragmented prior knowledge into traceable gene–homolog–marker–cell-type evidence chains, Xener extends plant cell-type annotation beyond species with well-developed reference atlases and supports comparative analyses of cellular identity across plant lineages.

Results

Xener integrates a plant cell-type KG with bidirectional evidence propagation

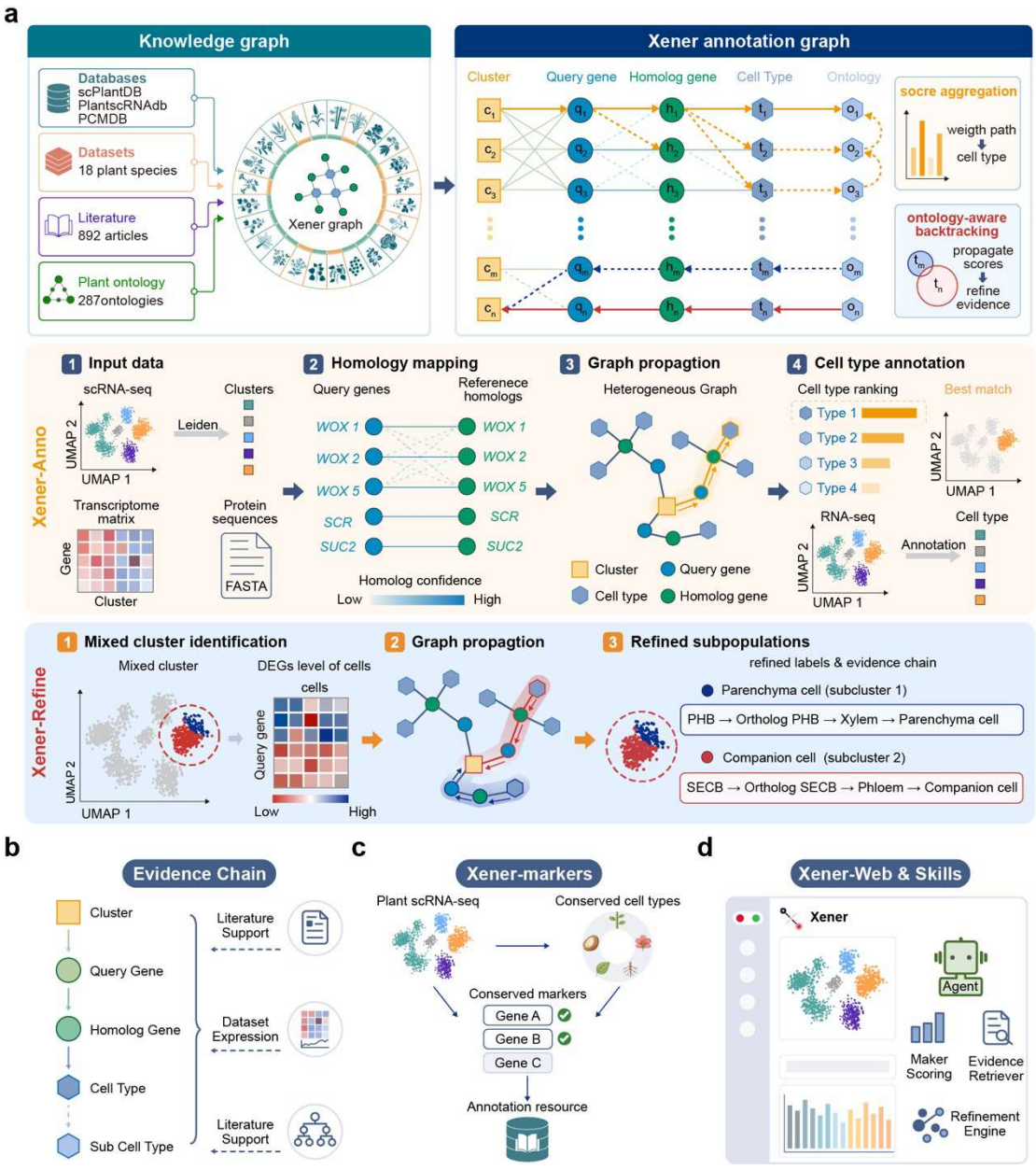
To address the challenges of cross-species cell-type annotation, we developed Xener, a reference-independent and knowledge-guided framework that integrates a plant cell-type KG with bidirectional evidence propagation (**Figure 1a, top panel**). The KG links DEGs from query clusters to homologous genes or orthogroups, curated marker–cell-type associations, and PO-standardized cell-type terms (Cooper et al., 2013; Walls et al., 2012). Two annotation modules operate on this graph: Xener-Anno propagates evidence from cluster-level DEGs toward candidate cell types (**Figure 1a, middle panel**), whereas Xener-Refine reverses this flow by projecting identity-specific evidence onto individual cells (**Figure 1a, bottom panel**). Together, Xener-Anno and Xener-Refine form the core computational framework, providing explicit and traceable paths from query-cluster DEGs to cell-type assignments. To facilitate practical use, Xener also provides a marker resource (Xener-Markers) and two user interfaces (Xener-Web and Xener-Skill).

To construct the KG, we assembled marker evidence from PCMDB (Jin et al., 2022), PlantscRNAdb (Chen et al., 2021), and scPlantDB (He et al., 2024), together with curated records from 892 publications **(Figure 1a; Supplementary Data Sets S1 and S2)**. The resulting resource contained 345,117 marker–cell-type association records across 18 species and 287 standardized PO terms. Each record retained its species, tissue, evidence type, and provenance, thereby harmonizing heterogeneous source nomenclature without discarding biological context (Tandon et al., 2026). Mapping markers to orthogroups further yielded 5,853 associations between orthogroups and cell types, allowing marker evidence from different species to be aggregated through shared gene families (Emms and Kelly, 2019; **Supplementary Data Set 3**).

For cluster-level annotation, Xener-Anno maps query-cluster DEGs to homologous genes or orthogroups and propagates their scores through weighted homology and marker–cell-type edges **(Figure 1a, middle panel)**. Path-dependent attenuation limits the contribution of longer or weaker evidence paths. Ontology-aware backtracking then selects the most specific PO term that meets the predefined discrimination criterion and stops at the last unambiguous term when no single child term qualifies **(see Methods)**. Each assignment retains a traceable chain linking query DEGs, cross-species homologs, marker associations, candidate cell types, and supporting records **(Figure 1b)**. Xener-Refine then projects candidate-specific gene contributions from the annotated cluster onto its constituent cells, evaluates this support against each cell's expression profile, and smooths the resulting scores over the within-cluster k-nearest-neighbor graph (Wolf et al., 2018). Because refinement is restricted to identities supported during cluster-level annotation, it can resolve evidence-supported subpopulations without introducing unrelated labels or requiring reclustering **(Figure 1a, bottom panel; Supplementary Figure S1)**.

In addition to annotation and refinement, Xener organizes standardized marker records by cell type and orthogroup into Xener-Markers, a reusable resource that links marker evidence across species through shared orthogroups **(Figure 1c)**. Xener-Web (https://xener.dcs.cloud) provides interactive access to annotation rankings, marker scoring, evidence retrieval, graph exploration, and subpopulation refinement. Xener-Skill, distributed with the source code (https://github.com/BGIResearch/Xener), provides structured interfaces that enable artificial intelligence (AI) agents to invoke Xener-Anno and Xener-Refine **(Figure 1d)**.

Figure 1. Xener integrates knowledge graph-guided annotation, evidence-supported refinement, and reusable marker resources across plant species.



a Xener comprises a plant cell-type KG, Xener-Anno, and Xener-Refine. The KG integrates marker associations from databases, published plant single-cell RNA-sequencing datasets, curated literature, and PO. Xener-Anno maps cluster DEGs to homologous genes and propagates weighted evidence to rank candidate cell types, followed by ontology-aware backtracking. Xener-Refine

projects candidate-specific gene evidence onto individual cells and resolves mixed clusters into evidence-supported subpopulations. **b** Conceptual schematic of the node and record types contributing to a traceable evidence chain, including query clusters and DEGs, cross-species homologs, cell types, ontology terms, and supporting literature, expression, and ontology records. This panel is a conceptual schematic rather than a direct export from a specific annotation run. **c** Xener-Markers organizes marker records across plant datasets, standardized cell types, and orthogroups into a reusable resource of cross-species, orthogroup-linked marker evidence. **d** Xener-Web provides interactive annotation, marker scoring, evidence retrieval, graph exploration, and subpopulation refinement, whereas Xener-Skill provides structured programmatic access to Xener-Anno and Xener-Refine for agent-based workflows. DEG, differentially expressed gene; KG, knowledge graph; PO, Plant Ontology.

Xener yields higher hierarchical concordance across the evaluated cross-species datasets

To evaluate cross-species cell-type annotation performance, we analyzed 62 publicly available single-cell dataset entries spanning 24 plant species and multiple organs **(Supplementary Data Set 4)**. We compared Xener with two other reference-independent methods, GPTCelltype (Hou and Ji, 2024) and a PubMed-SKILL-assisted workflow, and with SATURN (Rosen et al., 2024) as a reference-dependent cross-species label-transfer baseline (**Figure 2a–c)**. The three reference-

independent methods received identical inputs (the same query datasets, Leiden cluster partitions (Traag et al., 2019), DEG lists, and species and organ metadata), whereas SATURN used organ-matched *Arabidopsis thaliana* references. All methods were scored against the same benchmark labels using an identical PO-aware hierarchical-concordance criterion (see **Methods)**.

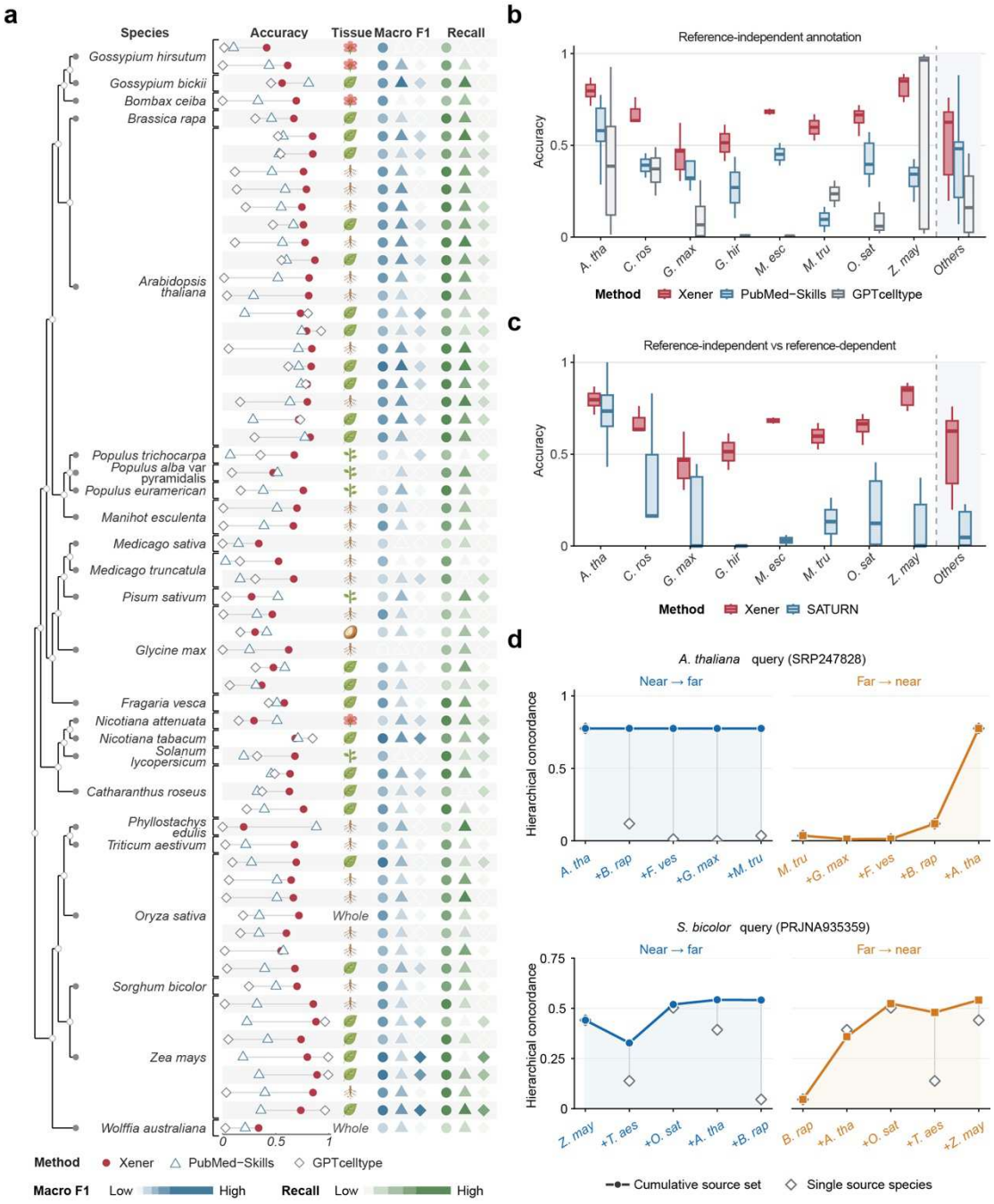
Xener showed the strongest overall performance in the reference-independent benchmark (**Figure 2a**). Its mean and median hierarchical concordance were 0.663 and 0.693, respectively, compared with 0.437 and 0.431 for PubMed-SKILL and 0.280 and 0.166 for GPTCelltype **(Supplementary Data Set 4)**. Xener ranked first for 46 of 62 entries and second for 15 entries. At the species level, Xener achieved the highest median concordance for 17 of 24 species (**Figure 2b**). Its concordance was also more stable than that of SATURN across the full cohort, with an interquartile range (IQR) of 0.186 versus 0.673 for SATURN. GPTCelltype and PubMed-SKILL showed smaller IQRs (0.415 and 0.245, respectively), but for GPTCelltype this narrow spread reflects uniformly low concordance rather than consistent accuracy (**Figure 2b; Supplementary Data Set 4)**.

Xener also outperformed the reference-dependent SATURN workflow (**Figure 2c**), achieving a median hierarchical concordance 3.47 times that of SATURN (0.693 versus 0.200; two-sided paired Wilcoxon signed-rank test, $P = 6.70 \times 10^{-9}$) and lower across-dataset variability **(Supplementary Data Set 4)**. Xener retained strong performance among nonmodel species with limited reference resources **(Supplementary Figure S2)**. For example, in the *Catharanthus roseus* leaf dataset SRP335448 (Li et al., 2023), Xener achieved a concordance of 0.635, compared with

0.457, 0.490, and 0.163 for PubMed-SKILL, GPTCelltype, and SATURN, respectively **(Supplementary Figure S3)**. The agent-based Xener-Skill interface also remained competitive, with a median hierarchical concordance of 0.498, corresponding to 1.16 times that of PubMed-SKILL and 3.00 times that of GPTCelltype (**Supplementary Figure S4**).

We next examined how the composition of knowledge-source species affected Xener annotation in model- and nonmodel-species queries (**Figure 2d, e; Supplementary Data Set 5**). With respect to the *A. thaliana* query, same-species knowledge alone yielded high concordance (0.776) and incorporating four additional source species in order of increasing phylogenetic distance neither improved nor degraded concordance (**Figure 2d**). In the reverse order, phylogenetically distant evidence alone yielded near-zero concordance until *A. thaliana* knowledge itself was added. Thus, the presence of same-species knowledge was available, it largely determined annotation performance, and additional cross-species evidence had little effect. The *S. bicolor* query represents the opposite, nonmodel setting, in which the KG contains no same-species records. Starting from the phylogenetically closest available relative (*Z. mays*; 0.441) gave a markedly higher initial concordance than starting from the distant *Brassica rapa* (0.046). As evidence from additional species accumulated, the two addition orders converged to the same concordance (0.541), despite intermediate fluctuations (**Figure 2e)**. By integrating evidence across multiple source species, Xener therefore supports the annotation of nonmodel plants without the need for requiring users to identify a single optimal reference species in advance.

Figure 2. Cross-species annotation benchmark and cumulative knowledge-source analysis.



a Dataset-level hierarchical-concordance scores across 62 single-cell dataset entries from 24 plant species. The left panel shows the accuracy comparison among Xener, PubMed-SKILL and GPTCelltype, with symbol shape and color identifying the annotation methods. Accuracy denotes PO-aware hierarchical concordance (see Methods). The middle and right panels show the

corresponding macro-F1 and recall values, encoded by fill gradients. Organ icons indicate the sampled tissue or organ. **b** Species-level distributions of hierarchical concordance for the three reference-independent methods. Each box summarizes the dataset-level scores for one species group. Species represented by a single dataset are pooled into Others for visualization. Species-group labels: A. tha, *Arabidopsis thaliana*; C. ros, *Catharanthus roseus*; G. max, *Glycine max*; G. hir, *Gossypium hirsutum*; M. esc, *Manihot esculenta*; M. tru, *Medicago truncatula*; O. sat, *Oryza sativa*; Z. may, *Zea mays*. Boxes indicate the IQR and median, and whiskers extend to 1.5 times the IQR. **c** Species-level distributions of hierarchical concordance for Xener and the reference-dependent SATURN across the same benchmark entries, displayed as in b. Each query dataset was evaluated by both methods. The between-method difference is reported in the text (two-sided paired Wilcoxon signed-rank test). **d** Cumulative knowledge-source analysis for the model plant *A. thaliana* SRP247828. **e** Cumulative knowledge-source analysis for the non-model plant *Sorghum bicolor* PRJNA935359. In d and e, source species were added one at a time in predefined near-to-far or far-to-near orders, and a separate annotation was completed after each cumulative addition. The x axis indicates the cumulative source-species series (five steps per order), and "+" marks the source species added at each step.

Xener enables evidence-supported and traceable cross-species cell-type annotation

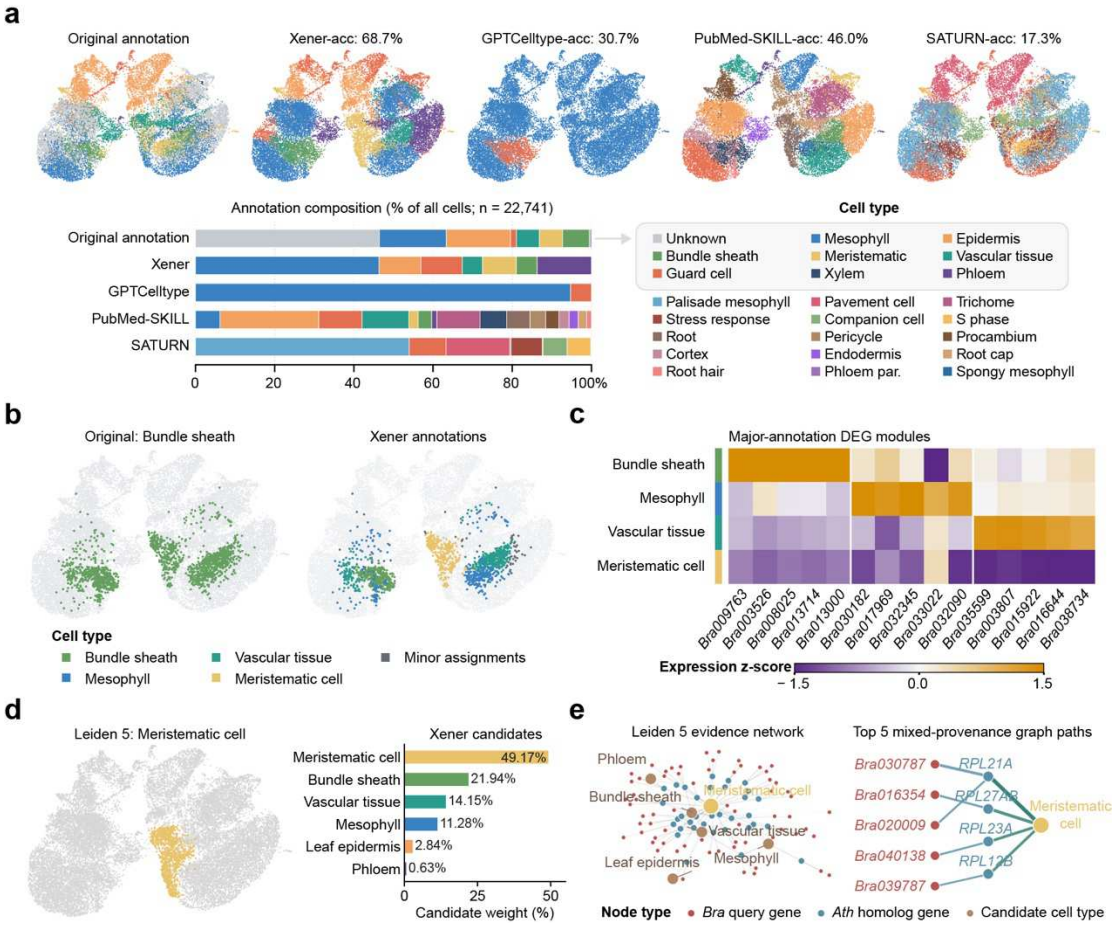
Xener annotates a query dataset by integrating its markers with cross-species homologous-gene and cell-type evidence, thereby producing ranked cell-type assignments that can be examined at both the gene and population levels. We applied this workflow to the *B. rapa* single-cell atlas CRA006988 (Guo et al., 2022) and compared the resulting annotations with those generated by GPTCelltype, PubMed-SKILL, and SATURN (**Figure 3a**). With the published atlas labels as the reference standard, 12,180 of the 22,741 profiled cells (53.6%) had defined cell-type annotations and could be evaluated. Among these cells, Xener showed 68.7% hierarchical concordance with the original atlas under the specified ontology-aware evaluation scheme, compared with 30.7% for GPTCelltype, 17.3% for SATURN, and 46.0% for PubMed-SKILL **(Supplementary Data Set 6)**. Xener also assigned the 10,561 cells originally labeled Unknown to candidate cell identities, dominated by Mesophyll (63.2%) and Phloem (15.5%), with the remaining cells distributed among epidermal, vascular, ground-tissue, and meristematic populations **(Supplementary Data Set 6)**.

In addition to assigning previously unresolved cells, Xener refined existing annotations. Among the 1,540 cells originally labeled Bundle sheath, Xener assigned 353 to Bundle sheath, 338 to Mesophyll candidates, 464 to Vascular tissue candidates, and 331 to Meristematic cell candidates, with 54 receiving minor assignments **(Figure 3b; Supplementary Data Set 7)**. These populations occupied distinct uniform manifold approximation and projection (UMAP; McInnes et al., 2018) regions and exhibited population-specific DEG modules **(Figure 3b, c)**. When nonoverlapping populations from the same dataset as internal references (**see Methods**), Mesophyll candidates were more strongly correlated with the Mesophyll reference than with the Vascular tissue reference (r =

0.857 versus 0.692). Vascular tissue candidates were more strongly correlated with the Vascular tissue reference than with the Mesophyll reference (r = 0.821 versus 0.788) **(Supplementary Data Set 7)**. Their separation in terms of shared embedding, distinct DEG modules, and identity-consistent correlations suggests that Xener resolved transcriptionally coherent candidate populations within a single broad atlas label.

The refined assignments retained the evidence underlying each decision. Among the 331 Meristematic cell candidates, 94.9% localized to Leiden cluster 5. Across the complete Leiden 5 cluster, Meristematic cell accounted for 49.17% of the normalized candidate evidence weight, compared with 21.94% for Bundle sheath **(Figure 3d)**. The corresponding evidence network connected query genes through *A. thaliana* homologs to six ranked candidate cell types **(Figure 3e)**. All five highest-scoring mixed-provenance paths supported Meristematic cell through distinct pairs of *B. rapa* query genes and their *A. thaliana* homologs, with combined path scores ranging from 9.30×10^4 to 2.96×10^5 and sequence identities ranging from 88.4% to 99.4% **(Supplementary Data Set 8)**. Together, the cluster-level candidate weights and quantitative gene–homolog–cell type paths provided a traceable and auditable basis for the Meristematic cell assignment.

Figure 3. Xener integrates cross-species evidence for cell-type annotation and within-cluster refinement.



a UMAPs and cell-type compositions for the original annotation and the annotations generated by Xener, GPTCelltype, PubMed-SKILL and SATURN. Hierarchical-concordance values are calculated among cells with known original annotations. **b** Resolution of the original Bundle sheath population by Xener. Minor assignments comprise Phloem, Leaf epidermis, Vascular tissue > Phloem and Guard cell. **c** Expression scores for representative differentially expressed gene modules associated with the major Xener-refined populations. **d** UMAP localization of Leiden cluster 5 and normalized cluster-level Xener candidate-evidence weights. **e** Leiden cluster 5

evidence architecture connecting *B. rapa* query genes to *A. thaliana* homologs and six candidate cell types. Path numbers indicate rank, and node colors denote query genes, *ATH* homologs and candidate cell types.

Xener identifies candidate cell-type markers conserved across plant lineages

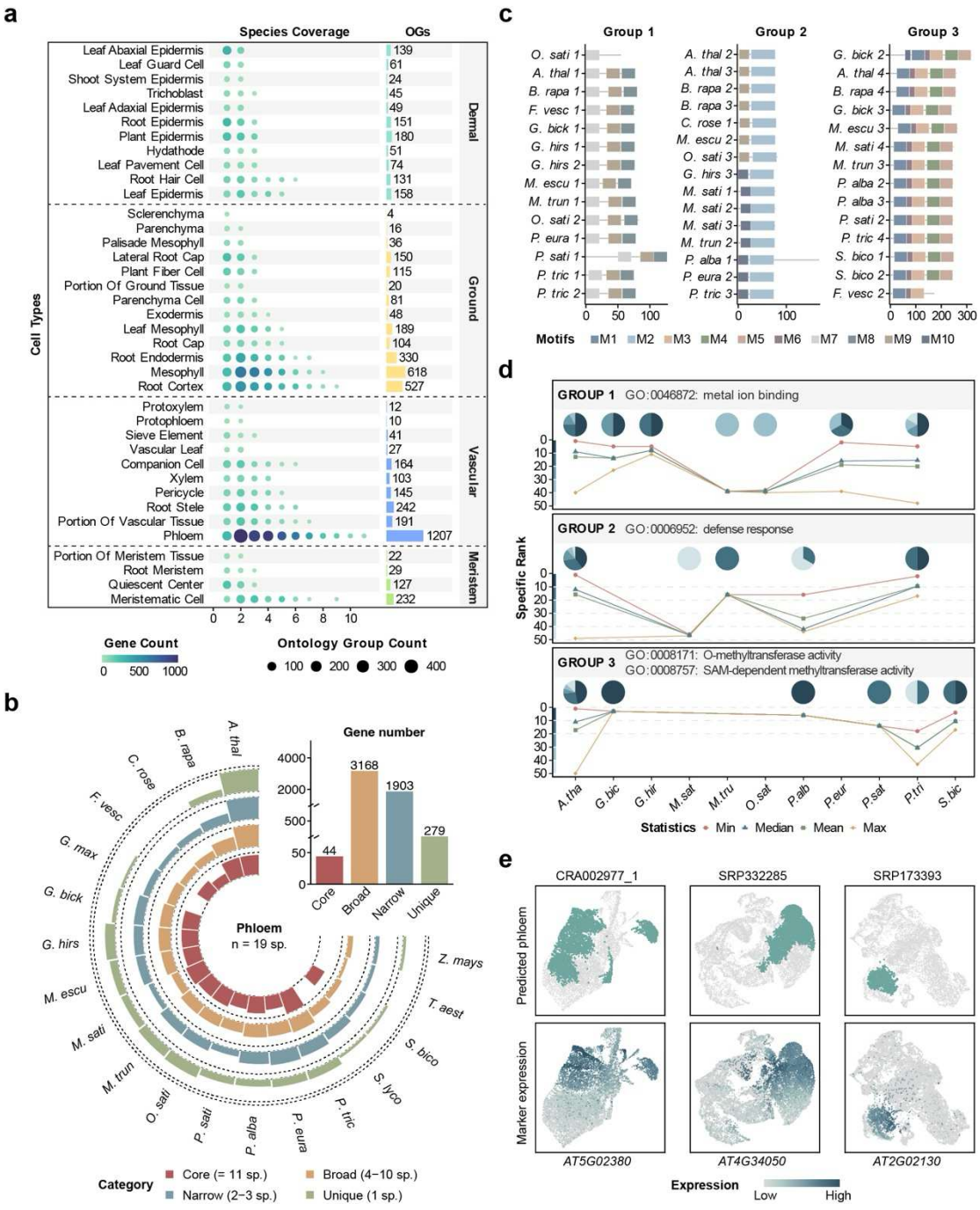
To characterize the conservation of Xener-supported candidate cell-type markers across plant lineages, we organized the retained annotation evidence into Xener-Markers, comprising 21,545 marker records from all 24 benchmark species. Of these, 21,516 records from 22 species were linked to orthogroups and included in the conservation analysis **(Figure 4a; Supplementary Data Set 3)**. The resulting resource contained 5,853 associations between orthogroups and 38 PO cell-type terms, including 11 dermal, 13 ground-tissue, 10 vascular, and 4 meristematic terms. These categories contained 1,063, 2,238, 2,142, and 410 associations, respectively. For each cell type, orthogroups were classified as Core, Broad, Narrow, or Unique according to their relative species coverage **(see Methods; Supplementary Figure S5)**. Across cell types, the maximum orthogroup coverage ranged from 1 to 11 species, with the phloem showing the broadest conservation across 11 species, followed by root cortex and meristematic cells across nine species each and the mesophyll across eight species.

Phloem, which showed the greatest maximum orthogroup coverage, contained 5,394 marker records linked to 1,207 orthogroups spanning 19 species in total (**Figure 4a, b)**. Among these

311 records, 44 were linked to Core orthogroups, 3,168 to Broad orthogroups, 1,903 to Narrow
312 orthogroups, and 279 to Unique orthogroups **(Figure 4b; Supplementary Data Set 9**). The 44
313 Core records represented 43 unique protein entries and collectively contained 10 recurring motifs
314 (Bailey et al., 2015). Their motif architectures separated the proteins into three groups associated
315 with metallothioneins, defensin/knottin-like proteins, and O-methyltransferases **(Figure 4c, d;**
316 **Supplementary Data Set 10)**. InterProScan-derived protein-family and GO annotations (Jones et
317 al., 2014) associated these groups with metal ion binding, defense response, and O-
318 methyltransferase activity, respectively, consistent with their reported roles in metal homeostasis,
319 defense, and phenylpropanoid and lignin metabolism (Yang et al., 2009; Seregin and Kozhevnikova,
320 2023; Parisi et al., 2019; Dixon and Barros, 2019).

321 The expression patterns of representative Core phloem markers were consistent with
322 enrichment in Xener-predicted phloem populations. The mean expression of *AT5G02380*,
323 *AT4G34050*, and *AT2G02130* was highest in the Xener-predicted phloem clusters in
324 CRA002977_1, SRP332285, and SRP173393, respectively **(Figure 4e)**. Their mean expression in
325 predicted phloem cells was 3.43-, 5.34-, and 22.82-fold higher than that in the remaining cells of
326 the corresponding datasets **(**two-sided Wilcoxon rank-sum tests, all BH-adjusted $P < 0.001$;
327 **Supplementary Data Set 11)**. Together, the orthogroup coverage and expression analyses
328 prioritize candidate phloem markers supported by both cross-lineage occurrence and cell
329 population-enriched expression (Chau et al., 2025; Xue et al., 2025).

Figure 4. Cross-species conservation and characterization of Xener-supported candidate cell-type markers.



a Species coverage of orthogroup-linked marker records across 38 standardized cell-type terms. Terms are grouped into dermal, ground-tissue, vascular, and meristematic categories. Bubble color

indicates the number of mapped marker records, and adjacent bars indicate the number of associated orthogroups. Marker records originated from 24 benchmark species, with orthogroup-linked records available for 22 species. **b** Phloem marker records classified as Core, Broad, Narrow, or Unique according to orthogroup species coverage across 19 species. The radial bar length is proportional to the square root of the record count. **c** Relative positions of 10 recurring motifs in Core phloem marker proteins. **d** InterProScan functional annotations and cross-species marker-rank summaries for the three motif-associated protein groups. Lines indicate the minimum, median, mean, and maximum rank for each species; lower ranks indicate higher marker specificity. **e** UMAPs showing Xener-predicted cell-type assignments and expression of *AT5G02380* in CRA002977_1, *AT4G34050* in SRP332285, and *AT2G02130* in SRP173393. Phloem-predicted populations are indicated in the upper panels, and expression of the corresponding marker is shown in the lower panels.

Xener-Refine distinguishes evidence-supported subpopulations within annotated clusters

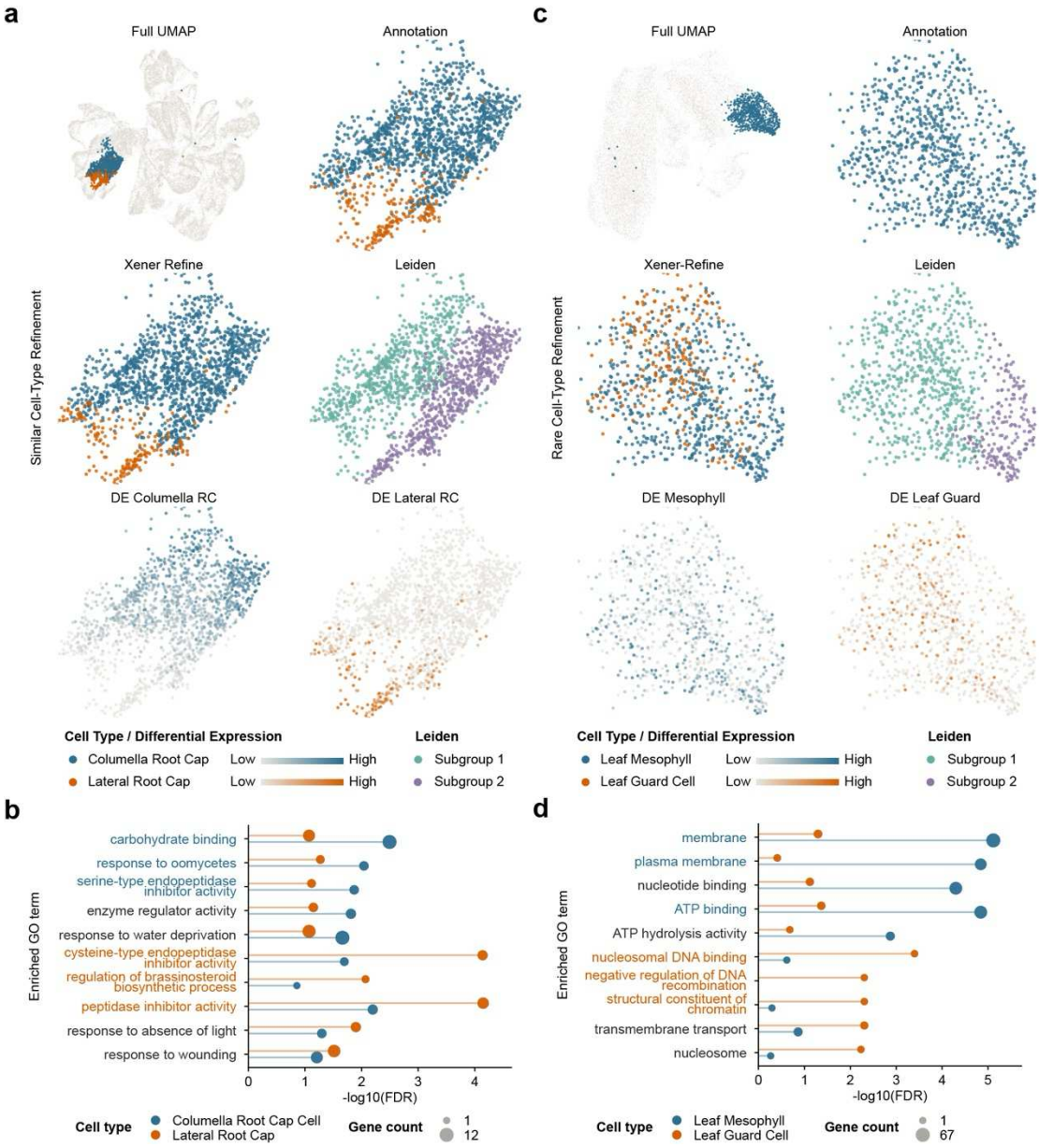
Xener-Refine projects candidate-specific graph evidence from an annotated cluster onto its constituent cells, enabling cell-level resolution of closely related identities supported by cluster-level annotation **(Figure 1a; Supplementary Figure S6)**. In the *A. thaliana* root dataset SRP171040 (Ryu et al., 2019), Leiden cluster 3 contained 1,589 cells with published columella and

lateral root cap labels, two closely related root cap identities **(Figure 5a)**. Xener-Refine assigned 1,388 cells to the columella root cap and 201 to the lateral root cap. Of these assignments, 1,315 and 159 matched the respective published labels, corresponding to agreement rates of 94.7% and 79.1%, respectively. All 42 disagreements among lateral root cap assignments corresponded to published columella root cap cells, and 36 (85.7%) were located at the boundary between the two populations in the expression UMAP **(Supplementary Data Set 12)**. Expression-only Leiden reclustering at a resolution of 0.1 produced subgroups of 866 and 723 cells, with published columella cells accounting for 89.8% and 80.1% of the respective subgroups. Both expression-defined subgroups therefore contained columella and lateral root cap cells. Columella-supporting genes were enriched for carbohydrate binding and response to oomycetes (false discovery rate (FDR) = 3.21×10^{-3} and 9.09×10^{-3}, respectively), and lateral-root-cap-supporting genes were enriched for peptidase inhibitor activity and regulation of brassinosteroid biosynthesis (FDR = 7.12×10^{-5} and 8.52×10^{-3}, respectively) **(Figure 5b; Supplementary Data Set 13)**. These results indicate that identity-specific graph evidence distinguished closely related root cap populations that remained mixed after expression-only reclustering at the tested resolution. Root-cap border cells are known to contribute to defense against soilborne pathogens, supporting the biological plausibility of oomycete-response enrichment (Fortier et al., 2023; Ropitaux et al., 2020).

Xener-Refine further revealed a candidate minority population embedded within a uniformly annotated cluster. In the *Z. mays* leaf dataset PRJNA662627 (Bezrutczyk et al., 2021), all 905 cells in Leiden cluster 4 were labeled mesophyll in the published annotation **(Figure 5c)**. Within the

cluster-level candidate set, Xener-Refine retained 674 cells as leaf mesophyll and assigned 231 cells to a candidate leaf guard cell-like identity through candidate-restricted graph scoring. Expression-only Leiden reclustering at a resolution of 0.2 generated subgroups of 691 and 214 cells, containing 215 and 16 candidate guard-cell-like assignments, respectively **(Figure 5c; Supplementary Data Set 12)**. The candidate cells therefore spanned both expression-defined subgroups, whereas graph-guided scoring localized guard-cell-associated evidence to a specific subset of cells. Their supporting genes showed enrichment for transmembrane transport. The full enrichment results additionally included regulation of intracellular pH and potassium ion transport (FDR = 4.95×10^{-3}, 7.47×10^{-3}, and 4.28×10^{-2}, respectively) **(Figure 5d; Supplementary Data Set 13)**.These transport-related functions were consistent with guard-cell biology and supported the prioritization of the graph-derived candidates, indicating that Xener-Refine can detect minority evidence signals obscured within a dominant cluster annotation (Zhang et al., 2024; De Angeli et al., 2013; Inoue et al., 2020).

Figure 5. Xener-Refine resolves cell-level heterogeneity within annotated clusters.



388

389 **a** Refinement of Leiden cluster 3 in the *Arabidopsis thaliana* root dataset SRP171040. The cluster

390 contained 1,589 cells with published columella root cap and lateral root cap labels. Xener-Refine

391 assigned 1,388 cells to columella root cap and 201 to lateral root cap; 1,315 and 159 assignments,

392 respectively, matched the corresponding published labels. Expression-only Leiden reclustering at

393 a resolution of 0.1 yielded subgroups of 866 and 723 cells, both containing columella root cap and

lateral root cap cells. **b** GO-enriched terms among genes supporting the two root cap assignments. **c** Refinement of Leiden cluster 4 in the *Zea mays* leaf dataset PRJNA662627. All 905 cells were labeled mesophyll in the published annotation. Xener-Refine retained 674 cells as leaf mesophyll and assigned 231 cells to a candidate leaf guard-cell-like identity. Expression-only Leiden reclustering at a resolution of 0.2 yielded subgroups of 691 and 214 cells, containing 215 and 16 candidate guard-cell-like assignments, respectively. **d** GO-enriched terms among genes supporting the leaf mesophyll and candidate leaf guard-cell-like assignments.

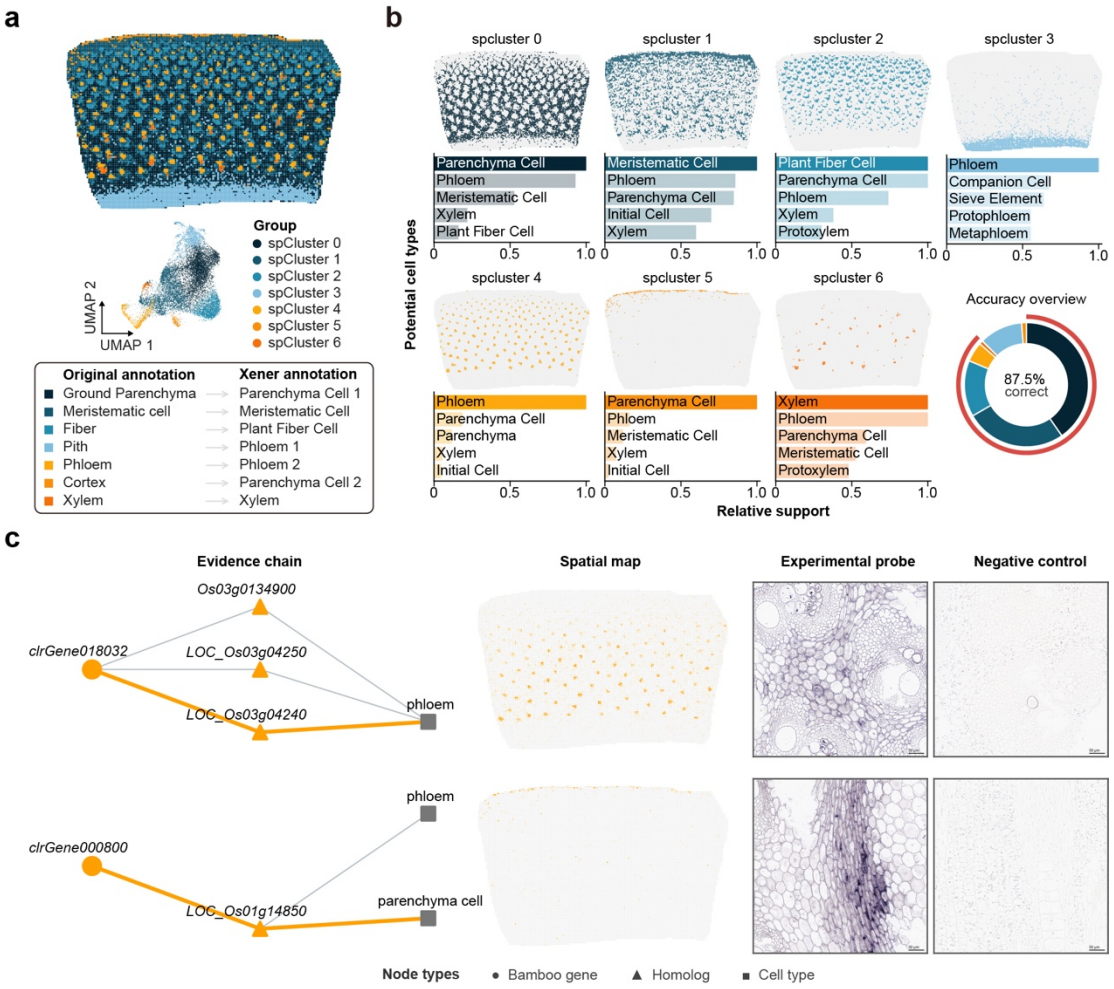
Xener identifies high-contribution markers and supports their spatial localization in Moso bamboo

We next asked whether the single-cell evidence used by Xener could be transferred to spatial annotation in a nonmodel plant. We applied Xener, using cell-type evidence from *A. thaliana* and *O. sativa*, to a bamboo (*Phyllostachys edulis*) spatial transcriptomic dataset (STDS0000377) generated during the rapid cell-division phase of the intercalary meristem (Qin et al., 2025). The dataset comprised 17,208 spots distributed across seven published spatial clusters, and the published bamboo labels were used only for post hoc evaluation. Xener-guided annotation followed by pairwise refinement recovered five published cluster identities, representing 15,050 of 17,208 spots and 87.5% spot-weighted agreement **(Figure 6a, b; Supplementary Data Set 14)**. This total included clusters 2 and 6: 2,354 of 2,520 spots in cluster 2 supported plant fiber cells rather than

parenchyma cells, and 167 of 169 spots in cluster 6 supported xylem rather than phloem **(Supplementary Data Set 15)**. Thus, in this dataset, evidence propagated from annotated single-cell datasets supported the recovery of spatially organized tissue identities in bamboo.

Xener also identified high-contribution genes underlying the spatial annotations. For example, *clrGene018032* and *clrGene000800* were among the leading contributors to spatial cluster 4 (sp-4; Phloem) and sp-5 (Cortex), respectively, with target-cluster detection fractions of 87.9% and 57.5% (**Figure 6c; Supplementary Data Set 16)**. *clrGene018032* linked through *LOC_Os03g04240* directly to Phloem, providing conserved identity-level support for sp-4. *clrGene000800* linked to parenchyma cell, capturing the parenchymatous composition and peripheral position of stem cortex and thereby supporting sp-5 at the anatomical level (Qin et al., 2025). Transverse RNA *in situ* hybridization revealed localized staining for both genes relative to their gene- and orientation-matched negative controls on the basis of one experimental section and one control section per gene (**Figure 6c; see Methods**). The staining quantification was descriptive. These results indicate that Xener can transfer cell-type evidence across species while revealing the high-contribution genes and biological relationships supporting each spatial assignment.

Figure 6. Xener transfers cross-species single-cell evidence to spatial annotation in Moso bamboo.



a Spatial organization of the seven published bamboo clusters, shown as the tissue map and cluster embedding. **b** Xener-guided candidate cell-type support and pairwise refinement across the spatial clusters; bars show the relative support of the displayed candidate cell types, with the final annotation highlighted. **c** Integrated evidence for two high-contribution marker candidates. The two rows correspond to *clrGene018032* associated with sp-4/Phloem and *clrGene000800* associated with sp-5/Cortex, with cluster labels referring to the published annotations. From left to right, each row shows the three-column gene–homolog–cell-type evidence network, the corresponding spatial map, a representative transverse RNA in situ hybridization field and its gene-matched negative

control. The *clrGene018032* network contains a direct path through *LOC_Os03g04240* to Phloem, whereas *clrGene000800* is linked through *LOC_Os01g14850* to parenchyma cell, the Xener-supported candidate identity for the cluster originally annotated as Cortex. Scale bars, 50 μm.

Discussion

Single-cell annotation across plant species is fundamentally an inference problem: A proposed identity must remain biologically meaningful despite gene family turnover, uneven reference coverage, and differences in annotation resolution (Birchler and Yang, 2022; Iohannes and Jackson, 2023). Xener addresses this problem by linking query expression, protein homology, curated marker knowledge, and the PO hierarchy in a traceable graph. Its main contribution is therefore not simply improved annotation concordance but an explicit representation of why a label is supported and when the evidence justifies only a broader identity. This distinction is important for the Plant Cell Atlas because comprehensive, tissue-matched reference atlases remain unavailable for many plant species (Rhaman et al., 2024; Nobori, 2025).

The behavior of Xener reflects how it combines evidence rather than any single marker or reference representation. Marker-rule methods interpret diagnostic genes (Pliner et al., 2019; Zhang et al., 2019; Shao et al., 2020; Ianevski et al., 2022), large language model (LLM)-based methods infer labels from marker lists (Hou and Ji, 2024), reference-mapping approaches transfer labels from established atlases (Aran et al., 2019; Kang et al., 2021; Lotfollahi et al., 2022), and cross-species embedding methods learn shared latent spaces (Rosen et al., 2024). These strategies can be

effective, but their predictions become difficult to evaluate when reference populations are incomplete, labels differ in granularity, or informative genes are connected through one-to-many homology. This problem is especially pronounced in plants, where whole-genome duplication, gene family expansion, and paralog subfunctionalization weaken simple one-to-one orthology (Panchy et al., 2016; Passalacqua and Gillis, 2024). Xener instead propagates expression evidence through multiple homology and marker-to-cell-type routes, downweights broadly connected markers, and uses ontology-guided backtracking when the evidence does not support a narrow label. Reverse projection then reuses the same supporting evidence to test whether a cluster contains distinct cellular identities. The framework does not eliminate ambiguity; it makes both the basis and the resolution of that ambiguity traceable.

The graph also provides a practical representation of cell identity as a layered evolutionary property rather than a fixed transcriptomic fingerprint. Homologous cell types may retain developmental position or physiological function even when individual markers are replaced, duplicated, or redistributed among paralogs (Arendt et al., 2016; Tarashansky et al., 2021; Guillotin et al., 2023). Single-cell profiling has further shown that leaf phloem comprises transcriptionally distinct cell types with specialized transport and metabolic functions (Kim et al., 2021; Bezrutczyk et al., 2021). Consistent with this view, the Core, Broad, Narrow, and Unique evidence classes captured different degrees of conservation across the species examined (Tung et al., 2023). In phloem, metallothionein-associated metal homeostasis, defensin/knottin-mediated defense, and O-methyltransferase-linked phenylpropanoid metabolism remained recognizable across divergent

lineages despite turnover in the contributing genes (Seregin and Kozhevnikova, 2023; Parisi et al., 2019; Dixon and Barros, 2019). Together with recent evidence that orthologous marker groups and coexpression preserve cell-type signals across plants (Passalacqua and Gillis, 2024; Chau et al., 2025), these results suggest that cross-species disagreement need not be treated only as annotation failure. It may instead identify programs that have been split, merged, or implemented through different molecular components, providing focused hypotheses for evolutionary and functional studies.

Xener nevertheless remains limited by the evidence encoded in its graph. Sequence-based protein homology cannot propagate signals from lineage-specific orphan genes, noncoding transcripts, or rapidly diverged proteins, and sparse marker curation can reduce confidence for specialized cell types. Structural protein similarity (Jumper et al., 2021; Lin et al., 2023) and cross-species coexpression could provide complementary edges where primary-sequence conservation has eroded, while phylogenetic weighting could distinguish support arising from recent ancestry from evidence retained across deeper lineages (Passalacqua and Gillis, 2024; Theodoris et al., 2023). A common developmental origin or equivalent function cannot be established by transcriptomic correspondence alone; chromatin accessibility, spatial organization, lineage information, and perturbation responses (Cao and Gao, 2022; Hao et al., 2021) are needed as independent tests of graph-derived identities (Dorrity et al., 2021; Farmer et al., 2021). The bamboo analysis illustrates both sides of this boundary: model-plant evidence could be transferred to a

distant grass species, whereas the remaining discordant clusters exposed gaps in reference coverage (Qin et al., 2025).

Several aspects of the present evaluation also warrant caution (Heumos et al., 2023). The KG aggregates published marker knowledge, so overlap between its source databases and some benchmark datasets cannot be fully excluded, and source-exclusion analyses would be needed to quantify any resulting inflation. The two reference-independent comparators were run through a single LLM backbone, and their measured performance partly reflects that choice of model and prompt. SATURN was likewise evaluated only with organ-matched *A. thaliana* references, the setting most commonly available in practice, and broader reference panels might narrow the observed gap (De Donno et al., 2023; Fischer et al., 2024). The sensitivity of annotation to propagation and backtracking parameters was not systematically explored. The RNA *in situ* hybridization validation involved limited biological replication and therefore provides qualitative rather than quantitative support. Finally, Xener-Markers is distilled from Xener's own annotations, and its entries should be treated as candidate markers pending independent validation. Xener should therefore be viewed not as a final arbiter of cell identity but as an evidence-traceable comparative coordinate system in which supported correspondences and unresolved uncertainty can guide continued atlas refinement.

Methods

Xener framework overview

The Xener suite consists of two analytical modules, Xener-Anno and Xener-Refine; a supporting cross-species marker resource, Xener-Markers; and two user-facing interfaces, Xener-Web and Xener-Skill, which are built around the standard AnnData data structure (Wolf et al., 2018). All analyses were performed using the released Xener package (v0.1.12) with the default runtime configuration, which retained the top 30 query markers per cluster after homolog mapping and used a path-mode decay factor of 0.7.

(i) Xener-Anno integrates orthology, protein homology, marker expression, curated cell-type identities and ontology relationships to annotate cell clusters. It reports the assigned label or ontology path, ranked candidates, gene-level contributions, and supporting evidence graph. (ii) Xener-Refine is a subpopulation refinement tool that uses the candidate cell-type rankings and gene-level contributions generated by Xener-Anno. It combines candidate marker scoring with neighborhood graph smoothing to achieve precise cell- or spot-level subdivision. (iii) Xener-Markers is an orthogroup-linked cross-species marker resource that organizes standardized marker records by cell type and classifies them as Core, Broad, Narrow, or Unique according to relative species coverage (see Construction of Xener-Markers). (iv) Xener-Web is a web-based tool built on Xener-Anno and Xener-Refine for annotation, refinement, and exploration of the results. It also visualizes conserved gene resources used for cell-type annotation. (v) Xener-Skill provides

structured input schemas that enable AI agents to invoke Xener-Anno and Xener-Refine and integrate Xener into automated workflows.

Knowledge graph construction and ontology harmonization

The plant cell-type marker records were compiled from PCMDB (Jin et al., 2022; accessed 2 February 2025) and PlantscRNAdb version 4.0 (accessed 2 February 2025) (Chen et al., 2021; Zheng et al., 2026). Additional marker records were obtained from scPlantDB (He et al., 2024; accessed 2 August 2026) and through manual curation of 892 published studies. Each record specified the species, organ or tissue, reported cell-type label, marker, evidence type, and source accession or citation. Duplicate associations were merged before graph construction, and reported labels were mapped to PO terms (accessed 13 February 2025) (Cooper et al., 2013; Walls et al., 2012). The resulting crosswalk retained standardized labels, ontology identifiers, and mapping status. Unmapped or ambiguous labels were excluded from automatic ontology assignment.

The graph comprised marker-gene, cell-type and ontology nodes connected by marker-to-cell-type associations and hierarchical ontology relationships. Each marker-to-cell-type association retained source provenance and a relation_confidence value of 1.0 for experimental evidence or 0.7 for computational evidence. During annotation, marker evidence was filtered by organ and reference species. Query genes were linked to reference-species markers through protein homology; the resulting evidence was then propagated through marker-to-cell-type associations and the ontology hierarchy.

Construction of Xener-Markers

For the Xener-Markers resource, retained marker records from the benchmark analyses were consolidated by species, dataset, standardized PO cell-type term, marker or protein identifier, and source evidence. The records were kept as distinct marker records for conservation summaries, whereas protein sequences were deduplicated only in preparation for the Core phloem motif analysis. The resulting resource comprised 21,545 marker records from 24 benchmark species; records with an orthogroup assignment were carried forward to the orthogroup-based conservation analysis described below.

Input data preprocessing

Benchmark expression data were acquired from AnnData objects, and cell and gene identifiers were made unique. When the maximum value of the expression matrix exceeded 1×10^5, genes detected in fewer than three cells and cells containing fewer than 200 detected genes were removed, followed by normalization to total count. Additionally, $log1p$ transformation was applied when the resulting maximum value exceeded 10. The same normalization and transformation criteria were applied to adata.raw when present. Highly variable gene selection was disabled. Existing dimensionality reduction, neighbor graph and cluster information was retained when available; missing components were generated by principal component analysis (PCA), k-nearest-neighbor graph construction, Leiden clustering (Traag et al., 2019) and UMAP (McInnes et al., 2018) using Scanpy (Wolf et al., 2018). Published cell-type labels were used only for evaluation.

Xener used the query expression object, cluster assignments, protein sequences, species, organ and reference-species settings. Cluster DEGs were retained when the log fold change was greater than 0.25, the Benjamini–Hochberg-adjusted *P* value was less than 0.05 and the gene was detected in more than 10% of cells in the focal cluster. GPTCelltype and PubMed-SKILL received cluster marker lists together with species and organ information through the DeepSeek-V4-Pro agent framework. SATURN received species-specific count matrices, protein embeddings and organ-matched labeled *A. thaliana* reference datasets. The *A. thaliana* reference datasets used for SATURN are listed in Supplementary Data Set 17.

Forward graph propagation for cluster-level cell-type annotation

For each query cluster, Xener initialized evidence at cluster-enriched DEG nodes as follows:

$$S_d^{(0)} = \mathrm{logFC}_d\left(\mathrm{pct}_{g,d} - \mathrm{pct}_{r,d}\right)[-\log_{10}(\mathrm{padj}_d)],$$

where logFC_d is the differential expression effect size, $\mathrm{pct}_{g,d}$ and $\mathrm{pct}_{r,d}$ are the expression fractions in the query cluster and reference group, respectively, and padj_d is the adjusted *P* value. Homologous gene and cell-type nodes were initialized to zero. DEG signals were propagated to homologous reference genes using protein-sequence identity-normalized weights:

$$w_{d,h} = \frac{\mathrm{pident}_{d,h}}{\sum_{h' \in H(d)} \mathrm{pident}_{d,h'}}.$$

The 30 homologous genes with the highest propagated signals were retained. Their signals were transferred to candidate cell types through normalized marker–cell-type association weights $w_{h,t}$. The homologs with broadly distributed associations were downweighted as follows:

$$r_h = 1.1 - \frac{\overline{a}_{h,\mathcal{T}}}{\max_t a_{h,t}},$$

where $\mathcal{T}(h)$ denotes the cell types associated with homolog h. The adjusted signals were aggregated at cell-type nodes to determine candidate annotation scores.

The cell type scores were further propagated from child to parent terms in the PO hierarchy as follows:

$$S_t^{\text{ont}} = S_t^{\text{local}} + \alpha \max_{c \in C(t)} S_c^{\text{ont}}, \alpha = 0.9,$$

where $C(t)$ denotes the children of ontology term t. Setting $\alpha = 0.9$ imposed a 10% attenuation at each ontology level. Starting from the highest-scoring candidate ontology term, Xener traversed toward more specific child ontology terms using softmax-normalized scores. Traversal continued when a single child exceeded the discrimination threshold of $\theta = 0.15$ and ontology traversal terminated at the last unambiguous ontology term when no child or multiple children exceeded the threshold.

Reverse graph projection for subpopulation refinement

Following cluster-level annotation, Xener projected cell-type evidence back to individual cells. For each annotated cell type t, the supporting query-gene set G_t was retrieved from the corresponding evidence paths. Cell-level support was calculated as follows:

$$S_{c,t}^{raw} = \frac{1}{|G_t|} \sum_{g \in G_t} x_{c,g},$$

where $x_{c,g}$ denotes the expression of gene g in cell c.

Raw support scores were smoothed over the within-cluster k-nearest neighbor graph defined by the Scanpy (v. 1.12.3; Wolf et al., 2018) connectivity matrix:

$$S_{c,t}^{smooth} = \frac{S_{c,t}^{raw} + \sum_{c' \in N(c)} S_{c',t}^{raw}}{|N(c)| + 1},$$

where $N(c)$ represents neighboring cells of cell c. Each cell was assigned to the cell type with the highest smoothed support score as follows:

$$t_c^* = \arg\max_t S_{c,t}^{smooth}.$$

Genes associated with each refined subpopulation were subjected to GO enrichment analysis (The Gene Ontology Consortium, 2023). Significant biological process, molecular function and cellular component terms were identified using multiple-testing-adjusted *P* values and summarized with their contributing gene counts. When benchmark labels were available, subpopulation purity was calculated as the proportion of cells matching the corresponding reference identity. Leiden reclustering was used as an expression-based comparator in mixed-population analyses.

Graph-based evidence tracing for interpretable annotation

Xener retained the composed evidence graph for each cluster, including propagated node weights, edge relation confidences and upstream source records. Candidate cell types were ranked by their accumulated propagated weights. Query gene–homolog–cell-type chains were reconstructed from the graph topology and visualized as candidate-specific supporting subgraphs. These chains

describe the computational provenance of each annotation and do not imply causal regulatory relationships.

Benchmarking and comparative evaluation

Benchmarking was conducted at the accession level across 62 dataset entries representing 24 plant species. Each accession was treated as an independent query dataset. Each dataset was analyzed using its query species and organ settings, while published cell-type labels were withheld during prediction and used only for evaluation. Xener, Xener-Skill, PubMed-SKILL and GPTCelltype were applied to the same query datasets without dataset-specific parameter tuning beyond these required inputs. Xener was run with a fixed graph-based annotation configuration. PubMed-SKILL and GPTCelltype were evaluated as reference-independent, knowledge-assisted workflows through the same agent framework using DeepSeek-V4-Pro. SATURN was evaluated separately using its recommended reference-dependent cross-species label transfer workflow (accessed 13 February 2025). Within each organ category, the same organ-matched *A. thaliana* reference datasets were used across query species. The SATURN reference accessions used for each organ category are listed in Supplementary Data Set 17.

Reference-composition sensitivity analysis was performed on *A. thaliana* SRP247828 and *Sorghum bicolor* PRJNA935359 using five candidate reference species per query. With respect to *A. thaliana*, the close-to-distant order was *A. thaliana*, *B. rapa*, *Fragaria vesca*, *Glycine max* and *Medicago truncatula*; the reverse order was used for distant-to-close addition. For *S. bicolor*, the

close-to-distant order was *Z. mays*, *T. aestivum*, *O. sativa*, *A. thaliana* and *B. rapa*; the reverse order was used for distant-to-close addition. References were added cumulatively, and all nonreference settings and the hierarchical-concordance scoring procedure were held fixed across configurations.

Benchmark scoring and performance metrics

For cluster-level annotations, the predicted label of each query cluster was assigned to all cells within that cluster and compared with the published cell-level labels. The predicted and published labels were standardized using the same PO crosswalk. A prediction was considered hierarchically concordant when the two labels were identical, had a parent–child relationship or shared the same immediate parent in the ontology. For each dataset, hierarchical-concordance accuracy was calculated as follows:

$$\text{Accuracy} = \frac{N_{\text{concordant}}}{N_{\text{evaluated}}},$$

where $N_{\text{concordant}}$ is the number of cells satisfying the hierarchical-concordance criteria and $N_{\text{evaluated}}$ is the total number of evaluated cells.

Precision, recall and F1 scores were calculated from the standardized published and predicted labels. For cell type k,

$$\text{Precision}_k = \frac{TP_k}{TP_k + FP_k},$$

$$\text{Recall}_k = \frac{TP_k}{TP_k + FN_k},$$

and

$$F1_k = \frac{2 \times \text{Precision}_k \times \text{Recall}_k}{\text{Precision}_k + \text{Recall}_k}.$$

Macroaveraged precision, recall and F1 scores were calculated as the unweighted means across the evaluable cell types. All the metrics were calculated separately for each dataset accession, and dataset-level scores were used for comparisons among the methods. Cells were not pooled across datasets for between-method statistical analyses. Between-method differences in dataset-level concordance were assessed with two-sided paired Wilcoxon signed-rank tests.

Orthogroup-based classification of cross-species marker evidence

Xener marker records were grouped by standardized cell type, and the corresponding protein sequences were assigned to orthogroups using OrthoFinder v2.5.5 (Emms and Kelly, 2019). Orthogroup membership was linked to the marker record, species, standardized cell type and protein identifier. Records without an orthogroup assignment were retained as unmapped and excluded from conservation classification.

For orthogroup o, species coverage k_o was defined as the number of benchmark species containing at least one orthogroup member associated with the focal cell type. Multiple members from the same species were counted once. For each cell type, the maximum species coverage was as follows:

$$M = \max_{o} k_o.$$

The lower threshold for the Broad category was defined as follows:

$$B = \max\{2, \min[\lceil \mathrm{mean}_o(k_o) \rceil, M - 1]\}.$$

When $M \leq 2$, B was set to M. Orthogroups were classified as Unique ($k_o \leq 1$), Narrow ($2 \leq k_o < B$), Broad ($B \leq k_o < M$) or Core ($k_o = M > 1$). Marker records inherited the category assigned to their corresponding orthogroups. Classification was performed separately for each standardized cell type.

Let n_k denote the number of orthogroups with species coverage k. The weighted mean species coverage was calculated as follows:

$$C_{\text{norm}} = \frac{\bar{k}_{\text{weighted}}}{24},$$

where 24 is the total number of benchmark species.

Core phloem marker structure and expression

Core phloem marker records were extracted from the orthogroup-based conservation classification, and their unique protein sequences were analyzed using MEME Suite v5.5.9 (Bailey et al., 2015). The identified motifs were designated M1–M10. Proteins were assigned to mutually exclusive motif architecture groups in a fixed order: Group 1 comprised proteins containing M7; Group 2 comprised proteins containing M2 together with M9 or M10, excluding proteins assigned to Group 1; and Group 3 comprised all remaining motif architectures. Protein family, domain and Gene Ontology (GO) annotations were obtained using InterProScan v5.78-109.0 (Jones et al., 2014) and summarized for each motif group.

The Core marker records were subsequently matched to cluster-specific differential expression results from the corresponding single-cell datasets. For each marker detected in a cluster

annotated as phloem by Xener, Specific_Rank recorded its position in the cluster-level differential expression ranking, with smaller values indicating higher-ranked markers. Rank distributions were summarized by motif group and species using the minimum, median, mean and maximum values, and the displayed summary values were divided by five to match the plot scale. Representative Core marker expression was extracted from the corresponding AnnData objects and visualized on UMAP embeddings together with the Xener cluster annotations.

For representative Core phloem markers, cluster-level mean expression was calculated within each corresponding AnnData object using the existing Leiden clusters. The peak-expression cluster was defined as the cluster with the highest mean expression of the marker. Cells in clusters whose Xener annotations exactly matched the phloem label were designated predicted-phloem cells, and all other cells formed the comparison group. The reported fold change was calculated as the mean expression across predicted-phloem cells divided by the mean expression across the remaining cells. The three representative marker–dataset pairs were selected when the peak-expression cluster was among the Xener-predicted phloem clusters.

Xener-Refine and expression-based analyses

Xener-Refine was applied after cluster-level Xener-Anno annotation using the candidate cell-type set returned for each focal cluster. For each focal cluster, cell-level support was projected from candidate-specific evidence paths, smoothed on the within-cluster Scanpy connectivity graph and converted to cell-level assignments by candidate-restricted argmax scoring. Both analyses used all

available candidate markers and split_method='argmax'. Moran's I–based marker filtering was disabled by setting moranI_threshold=-2, an out-of-range sentinel value. The SRP171040 *Arabidopsis* root analysis used Leiden cluster 3, columella root cap cell and lateral root cap as candidate identities; expression-only Leiden reclustering was restricted to this cluster at a resolution of 0.1. The PRJNA662627 maize leaf analysis used Leiden cluster 4, leaf mesophyll and leaf guard cell as candidate identities, the same refinement settings and expression-only Leiden reclustering restricted to this cluster at a resolution of 0.2. GO enrichment was computed for each refined subpopulation from its supporting gene set using one-sided Fisher's exact tests against the species-matched GO background, followed by Benjamini–Hochberg correction (Benjamini and Hochberg, 1995). Homolog-based GO transfer for the maize analysis used the documented best *O. sativa* homologs identified with BLAST+ (v2.16.0) (Camacho et al., 2009); analysis thresholds are recorded in the accompanying provenance files. Cell counts, subgroup compositions and enriched GO terms are provided in Supplementary Data Sets S12 and S13.

Spatial-transcriptomic annotation of bamboo

The preprocessed Moso bamboo spatial transcriptomic dataset STDS0000377 was obtained from the CNGB Spatial Transcriptomics Data Portal (https://db.cngb.org/stomics/datasets/STDS0000377). The dataset contained 17,208 spots and seven published spatial clusters. For the RNA *in situ* hybridization target analysis, sp-4 (Phloem) and sp-5 (Cortex) were treated as predefined anatomical targets, and *clrGene018032* and

clrGene000800 were evaluated as their corresponding spatially enriched candidate genes. Cross-species evidence was generated with *A. thaliana* and *O. sativa* references using percent identity >50, bit score >75, E value <0.05, top_num=5, node annotation mode, ann_strict=0, mapping_strict=0 and decay_factor=0.7. A single-best-homolog graph was used to test direct gene–homolog–target-label paths, whereas a top-five multihomolog graph was used to rank anatomy-supporting gene contributions.

For targets without a direct homolog-to-anatomical-label marker edge, the directly supported KG term was connected to the predefined anatomical label by the shortest path of up to four ontology steps using is_a, part_of, intersection_of or develops_from relations. Each stored ontology edge retained its original direction; reverse traversal during path finding did not reverse the biological direction represented in the graph. For each target, spatial-expression specificity, marker-weight rank, direct KG support and ontology-bridge evidence were summarized (Supplementary Data Sets S14 and S15).

RNA in situ hybridization and image analysis

RNA *in situ* hybridization fields were selected for tissue continuity, section integrity, focus and interpretable staining. For each candidate gene, one transverse and one longitudinal experimental-probe slide and corresponding gene-matched and orientation-matched negative control slides were analyzed. Slides were scanned at 20× with an approximate pixel resolution of 0.274 μm per pixel and read from MRXS-format image pyramids using OpenSlide (v4.0.0) (Goode et al., 2013).

Quantification was performed within the scanner-defined OpenSlide tissue bounds at approximately 16-fold downsampling. Pure-black unavailable pixels were excluded from the scan-valid region. Red–green–blue (RGB) pixels were converted to CIE L*a*b* (CIELAB) color space. A joint blue–purple score was calculated as sqrt(max(a*,0) × max(−b*,0)). The primary threshold was 2.5 CIELAB units; the sensitivity thresholds were 1.5, 2.0, 2.5, 3.0 and 3.5. For each analyzed slide, the fraction of scan-valid pixels above the threshold and descriptive color-score summaries were calculated. Experimental-minus-control differences were calculated as matched-slide sensitivity descriptors. No inferential statistics were performed. Transverse and longitudinal sections were analyzed as complementary views.

Data Availability

All single-cell RNA sequencing datasets analyzed in this study are publicly available from PlantscRNAdb and scPlantDB, with accession numbers listed in Supplementary Data Set 4. The benchmark results are available at https://zenodo.org/record/21483515. The cross-species marker resource Xener-Markers is accessible through the Xener web platform at https://xener.dcs.cloud.

Code Availability

The Xener source code, including Xener-Anno for cell-type annotation, Xener-Refine for subpopulation refinement, and Xener-Skill for AI-agent-assisted workflows https://github.com/BGIResearch/Xener. The web platform at https://xener.dcs.cloud provides interactive access to cell-type annotation, subpopulation refinement, and supporting evidence.

Funding Declaration

This work received funding from the National Natural Science Foundation of China (32430072 and 32271975 to H. Zhao) and the Research and Demonstration of Key Technologies for "Bamboo as Substitutes for Plastic" in Pilot Member States of the International Bamboo and Rattan Organization (to H. Zhao).

Competing Interest

L.C and S.F are named inventors on granted Chinese patent CN121415883B (application No. 202511884187.0), which relates to the cell annotation methodology described in this study. The remaining authors declare no competing interests.

References

1. Aran, D., Looney, A.P., Liu, L., Wu, E., Fong, V., Hsu, A., Chak, S., Naikawadi, R.P., Wolters, P.J., Abate, A.R., Butte, A.J. and Bhattacharya, M. (2019). Reference-based analysis of lung single-cell sequencing reveals a transitional profibrotic macrophage. Nature Immunology **20**: 163-172.

2. Arendt, D., Musser, J.M., Baker, C.V.H., Bergman, A., Cepko, C., Erwin, D.H., Pavlicev, M., Schlosser, G., Widder, S., Laubichler, M.D. and Wagner, G.P. (2016). The origin and evolution of cell types. Nature Reviews Genetics **17**: 744-757.

3. Bailey, T.L., Johnson, J., Grant, C.E. and Noble, W.S. (2015). The MEME Suite. Nucleic Acids Research **43**: W39-W49.

4. Benjamini, Y. and Hochberg, Y. (1995). Controlling the False Discovery Rate: A Practical and Powerful Approach to Multiple Testing. Journal of the Royal Statistical Society Series B: Statistical Methodology **57**: 289-300.

5. Bezrutczyk, M., Zöllner, N.R., Kruse, C.P.S., Hartwig, T., Lautwein, T., Köhrer, K., Frommer, W.B. and Kim, J.-Y. (2021). Evidence for phloem loading via the abaxial bundle sheath cells in maize leaves. The Plant Cell **33**: 531-547.

6. Birchler, J.A. and Yang, H. (2022). The multiple fates of gene duplications: Deletion, hypofunctionalization, subfunctionalization, neofunctionalization, dosage balance constraints, and neutral variation. The Plant Cell **34**: 2466-2474.

7. Camacho, C., Coulouris, G., Avagyan, V., Ma, N., Papadopoulos, J., Bealer, K. and Madden, T.L. (2009). BLAST+: architecture and applications. BMC Bioinformatics **10**: 421.

8. Cao, Z.-J. and Gao, G. (2022). Multi-omics single-cell data integration and regulatory inference with graph-linked embedding. Nature Biotechnology **40**: 1458-1466.

9. Chau, T.N., Timilsena, P.R., Bathala, S.P., Kundu, S., Bargmann, B.O.R. and Li, **S.** (2025). Orthologous marker groups reveal broad cell identity conservation across plant single-cell transcriptomes. Nature Communications **16**: 201.

10. Chen, H., Yin, X., Guo, L., Yao, J., Ding, Y., Xu, X., Liu, L., Zhu, Q.H., Chu, Q. and Fan, L. (2021). PlantscRNAdb: A database for plant single-cell RNA analysis. Molecular Plant **14**: 855-857.

11. Cheng, C., Chen, W., Jin, H. and Chen, X. (2023). A review of single-cell RNA-seq annotation, integration, and cell–cell communication. Cells **12**: 1970.

12. Clarke, Z.A., Andrews, T.S., Atif, J., Pouyabahar, D., Innes, B.T., MacParland, S.A. and Bader, G.D. (2021). Tutorial: guidelines for annotating single-cell transcriptomic maps using automated and manual methods. Nature Protocols **16**: 2749-2764.

13. Cooper, L., Walls, R.L., Elser, J., Gandolfo, M.A., Stevenson, D.W., Smith, B., Preece, J., Athreya, B., Mungall, C.J., Rensing, S., Hiss, M., Lang, D., Reski, R., Berardini, T.Z., Li, D., Huala, E., Schaeffer, M., Menda, N., Arnaud, E., Shrestha, R., Yamazaki, Y. and Jaiswal, P. (2013). The Plant Ontology as a tool for comparative plant anatomy and genomic analyses. Plant and Cell Physiology **54**: e1.

14. De Angeli, A., Zhang, J., Meyer, S. and Martinoia, E. (2013). AtALMT9 is a malate-activated vacuolar chloride channel required for stomatal opening in *Arabidopsis*. Nature Communications **4**: 1804.

15. De Donno, C., Hediyeh-Zadeh, S., Moinfar, A.A., Wagenstetter, M., Zappia, L., Lotfollahi, M. and Theis, F.J. (2023). Population-level integration of single-cell datasets enables multi-scale analysis across samples. Nature Methods **20**: 1683-1692.

16. Denyer, T., Ma, X., Klesen, S., Scacchi, E., Nieselt, K. and Timmermans, M.C.P. (2019). Spatiotemporal Developmental Trajectories in the *Arabidopsis* Root Revealed Using High-Throughput Single-Cell RNA Sequencing. Developmental Cell **48**: 840-852.e5.

17. Dixon, R.A. and Barros, J. (2019). Lignin biosynthesis: old roads revisited and new roads explored. Open Biology **9**: 190215.

18. Dorrity, M.W., Alexandre, C.M., Hamm, M.O., Vigil, A.L., Fields, S., Queitsch, C. and Cuperus, J.T. (2021). The regulatory landscape of *Arabidopsis thaliana* roots at single-cell resolution. Nature Communications **12**: 3334.

19. Emms**,** D.M. and Kelly, S. (2019). OrthoFinder: phylogenetic orthology inference for comparative genomics. Genome Biology **20**: 238.

20. Farmer, A., Thibivilliers, S., Ryu, K.H., Schiefelbein, J. and Libault, M. (2021). Single-nucleus RNA and ATAC sequencing reveals the impact of chromatin accessibility on gene expression in *Arabidopsis* roots at the single-cell level. Molecular Plant **14**: 372-383.

21. Fischer, F., Fischer, D.S., Mukhin, R., Isaev, A., Biederstedt, E., Villani, A.-C. and Theis, F.J. (2024). scTab: Scaling cross-tissue single-cell annotation models. Nature Communications **15**: 6611.

22. Fortier, M., Lemaitre, V., Gaudry, A., Pawlak, B., Driouich, A., Follet-Gueye, M.L. and Vicré, M. (2023). A fine-tuned defense at the pea root caps: Involvement of border cells and arabinogalactan proteins against soilborne diseases. Frontiers in Plant Science **14**: 1132132.

23. Goode, A., Gilbert, B., Harkes, J., Jukic, D. and Satyanarayanan, M. (2013). OpenSlide: A vendor-neutral software foundation for digital pathology. Journal of Pathology Informatics **4**: 27.

24. Guillotin, B., Rahni, R., Passalacqua, M., Mohammed, M.A., Xu, X., Raju, S.K., Ramírez, C.O., Jackson, D., Groen, S.C., Gillis, J. and Birnbaum, K.D. (2023). A pan-grass transcriptome reveals patterns of cellular divergence in crops. Nature **617**: 785-791.

25. Guo, X., Liang, J., Lin, R., Zhang, L., Zhang, Z., Wu, J. and Wang, X. (2022). Single-cell transcriptome reveals differentiation between adaxial and abaxial mesophyll cells in *Brassica rapa*. Plant Biotechnology Journal **20**: 2233-2235.

26. Hao, Y., Hao, S., Andersen-Nissen, E., Mauck, W.M., Zheng, S., Butler, A., Lee, M.J., Wilk, A.J., Darby, C., Zager, M., Hoffman, P., Stoeckius, M., Papalexi, E., Mimitou, E.P., Jain, J., Srivastava, A., Stuart, T., Fleming, L.M., Yeung, B., Rogers, A.J., McElrath, J.M., Blish, C.A., Gottardo, R., Smibert, P. and Satija, R. (2021). Integrated analysis of multimodal single-cell data. Cell **184**: 3573-3587.e29.

27. He, Z., Luo, Y., Zhou, X., Zhu, T., Lan, Y. and Chen, D. (2024). scPlantDB: a comprehensive database for exploring cell types and markers of plant cell atlases. Nucleic Acids Research **52**: D1629-D1638.

28. Heumos, L., Schaar, A.C., Lance, C., Litinetskaya, A., Drost, F., Zappia, L., Lücken, M.D., Strobl, D.C., Henao, J., Curion, F., Aliee, H., Ansari, M., Badia-i-Mompel, P., Büttner, M., Dann, E., Dimitrov, D., Dony, L., Frishberg, A., He, D., Hediyeh-zadeh, S., Hetzel, L., Ibarra, I.L., Jones, M.G., Lotfollahi, M., Martens, L.D., Müller, C.L., Nitzan, M., Ostner, J., Palla, G., Patro, R., Piran, Z., Ramírez-Suástegui, C., Saez-Rodriguez, J., Sarkar, H., Schubert, B., Sikkema, L., Srivastava, A., Tanevski, J., Virshup, I., Weiler, P., Schiller, H.B. and Theis, F.J.

(2023). Best practices for single-cell analysis across modalities. Nature Reviews Genetics **24**: 550-572.

29. Hou, W. and Ji, Z. (2024). Assessing GPT-4 for cell type annotation in single-cell RNA-seq analysis. Nature Methods **21**: 1462-1465.

30. Ianevski, A., Giri, A.K. and Aittokallio, T. (2022). Fully-automated and ultra-fast cell-type identification using specific marker combinations from single-cell transcriptomic data. Nature Communications **13**: 1246.

31. Inoue, S.I., Kaiserli, E., Zhao, X., Waksman, T., Takemiya, A., Okumura, M., Takahashi, H., Seki, M., Shinozaki, K., Endo, Y., Sawasaki, T., Kinoshita, T., Zhang, X., Christie, J.M. and Shimazaki, K.I. (2020). CIPK23 regulates blue light-dependent stomatal opening in *Arabidopsis thaliana*. The Plant Journal **104**: 679-692.

32. Iohannes, S.D. and Jackson, D. (2023). Tackling redundancy: genetic mechanisms underlying paralog compensation in plants. New Phytologist **240**: 1381-1389.

33. Jin, J., Lu, P., Xu, Y., Tao, J., Li, Z., Wang, S., Yu, S., Wang, C., Xie, X., Gao, J., Chen, Q., Wang, L., Pu, W. and Cao, P. (2022). PCMDB: a curated and comprehensive resource of plant cell markers. Nucleic Acids Research **50**: D1448-D1455.

34. Jones, P., Binns, D., Chang, H.Y., Fraser, M., Li, W., McAnulla, C., McWilliam, H., Maslen, J., Mitchell, A., Nuka, G., Pesseat, S., Quinn, A.F., Sangrador-Vegas, A., Scheremetjew, M., Yong, S.Y., Lopez, R. and Hunter, S. (2014). InterProScan 5: genome-scale protein function classification. Bioinformatics **30**: 1236-1240.

35. Jumper, J., Evans, R., Pritzel, A., Green, T., Figurnov, M., Ronneberger, O., Tunyasuvunakool, K., Bates, R., Žídek, A., Potapenko, A., Bridgland, A., Meyer, C., Kohl, S.A.A., Ballard, A.J., Cowie, A., Romera-Paredes, B., Nikolov, S., Jain, R., Adler, J., Back, T., Petersen, S., Reiman, D., Clancy, E., Zielinski, M., Steinegger, M., Pacholska, M., Berghammer, T., Bodenstein, S., Silver, D., Vinyals, O., Senior, A.W., Kavukcuoglu, K., Kohli, P. and Hassabis, D. (2021). Highly accurate protein structure prediction with AlphaFold. Nature **596**: 583-589.

36. Kang, J.B., Nathan, A., Weinand, K., Zhang, F., Millard, N., Rumker, L., Moody, D.B., Korsunsky, I. and Raychaudhuri, S. (2021). Efficient and precise single-cell reference atlas mapping with Symphony. Nature Communications **12**: 5890.

37. Ke, Y., Pujol, V., Staut, J., Pollaris, L., Seurinck, R., Eekhout, T., Grones, C., Saura-Sanchez, M., Van Bel, M., Vuylsteke, M., Ariani, A., Liseron-Monfils, C., Vandepoele, K., Saeys, Y. and De Rybel, B. (2025). A single-cell and spatial wheat root atlas with cross-species annotations delineates conserved tissue-specific marker genes and regulators. Cell Reports **44**: 115240.

38. Kim, J.Y., Symeonidi, E., Pang, T.Y., Denyer, T., Weidauer, D., Bezrutczyk, M., Miras, M., Zöllner, N., Hartwig, T., Wudick, M.M., Lercher, M., Chen, L.Q., Timmermans, M.C.P. and Frommer, W.B. (2021). Distinct identities of leaf phloem cells revealed by single cell transcriptomics. The Plant Cell **33**: 511-530.

913 39. Lee, T.A., Illouz-Eliaz, N., Nobori, T., Xu, J., Jow, B., Nery, J.R. and Ecker, J.R. (2025). A
914 single-cell, spatial transcriptomic atlas of the *Arabidopsis* life cycle. Nature Plants **11**: 1960-
915 1975.
916 40. Li, C., Wood, J.C., Vu, A.H., Hamilton, J.P., Rodriguez Lopez, C.E., Payne, R.M.E., Serna
917 Guerrero, D.A., Gase, K., Yamamoto, K., Vaillancourt, B., Caputi, L., O'Connor, S.E. and
918 Robin Buell, C. (2023). Single-cell multi-omics in the medicinal plant *Catharanthus roseus*.
919 Nature Chemical Biology **19**: 1031-1041.
920 41. Lin, Z., Akin, H., Rao, R., Hie, B., Zhu, Z., Lu, W., Smetanin, N., Verkuil, R., Kabeli, O.,
921 Shmueli, Y., dos Santos Costa, A., Fazel-Zarandi, M., Sercu, T., Candido, S. and Rives, A.
922 (2023). Evolutionary-scale prediction of atomic-level protein structure with a language model.
923 Science **379**: 1123-1130.
924 42. Liu, X., Shen, Q. and Zhang, S. (2023). Cross-species cell-type assignment from single-cell
925 RNA-seq data by a heterogeneous graph neural network. Genome Research **33**: 96-111.
926 43. Lotfollahi, M., Naghipourfar, M., Luecken, M.D., Khajavi, M., Büttner, M., Wagenstetter, M.,
927 Avsec, Ž., Gayoso, A., Yosef, N., Interlandi, M., Rybakov, S., Misharin, A.V. and Theis, F.J.
928 (2022). Mapping single-cell data to reference atlases by transfer learning. Nature
929 Biotechnology **40**: 121-130.
930 44. Marand, A.P., Chen, Z., Gallavotti, A. and Schmitz, R.J. (2021). A cis-regulatory atlas in
931 maize at single-cell resolution. Cell **184**: 3041-3055.e21.

45. McInnes, L., Healy, J., Saul, N. and Großberger, L. (2018). UMAP: Uniform Manifold Approximation and Projection. Journal of Open Source Software **3**: 861.

46. Nobori, T. (2025). Exploring the untapped potential of single-cell and spatial omics in plant biology. New Phytologist **247**: 1098-1116.

47. Panchy, N., Lehti-Shiu, M. and Shiu, S.H. (2016). Evolution of Gene Duplication in Plants. Plant Physiology **171**: 2294-2316.

48. Parisi, K., Shafee, T.M.A., Quimbar, P., van der Weerden, N.L., Bleackley, M.R. and Anderson, M.A. (2019). The evolution, function and mechanisms of action for plant defensins. Seminars in Cell & Developmental Biology **88**: 107-118.

49. Passalacqua, M.J. and Gillis, J. (2024). Coexpression enhances cross-species integration of single-cell RNA sequencing across diverse plant species. Nature Plants **10**: 1075-1080.

50. Pliner, H.A., Shendure, J. and Trapnell, C. (2019). Supervised classification enables rapid annotation of cell atlases. Nature Methods **16**: 983-986.

51. Qin, N., Liu, X., Li, S., Sun, L., Chen, C., Lou, W., Wang, X., Bao, P., Cao, B., Zhang, H., Gan, J., Hou, Y., Fan, Z., Liu, J., Wang, Y., Yang, H. and Zhao, H. (2025). Single-nucleus and spatial transcriptomics reveal the cell populations of intercalary meristems in bamboo. Proceedings of the National Academy of Sciences **122**: e2511701122.

52. Rhaman, M.S., Ali, M., Ye, W. and Li, B. (2024). Opportunities and challenges in advancing plant research with single-cell omics. Genomics, Proteomics & Bioinformatics **22**: qzae026.

53. Rhee, S.Y., Birnbaum, K.D. and Ehrhardt, D.W. (2019). Towards Building a Plant Cell Atlas. Trends in Plant Science **24**: 303-310.

54. Ropitaux, M., Bernard, S., Schapman, D., Follet-Gueye, M.-L., Vicré, M., Boulogne, I. and Driouich, A. (2020). Root Border Cells and Mucilage Secretions of Soybean, G*lycine Max* (Merr) L.: Characterization and Role in Interactions with the Oomycete *Phytophthora Parasitica*. Cells **9**: 2215.

55. Rosen, Y., Brbić, M., Roohani, Y., Swanson, K., Li, Z. and Leskovec, J. (2024). Toward universal cell embeddings: integrating single-cell RNA-seq datasets across species with SATURN. Nature Methods **21**: 1492-1500.

56. Ryu, K.H., Huang, L., Kang, H.M. and Schiefelbein, J. (2019). Single-Cell RNA Sequencing Resolves Molecular Relationships Among Individual Plant Cells. Plant Physiology **179**: 1444-1456.

57. Ryu, K.H., Zhu, Y. and Schiefelbein, J. (2021). Plant Cell Identity in the Era of Single-Cell Transcriptomics. Annual Review of Genetics **55**: 479-496.

58. Seregin, I.V. and Kozhevnikova, A.D. (2023). Phytochelatins: sulfur-containing metal(loid)-chelating ligands in plants. International Journal of Molecular Sciences **24**: 2430.

59. Seyfferth, C., Renema, J., Wendrich, J.R., Eekhout, T., Seurinck, R., Vandamme, N., Blob, B., Saeys, Y., Helariutta, Y., Birnbaum, K.D. and De Rybel, B. (2021). Advances and Opportunities in Single-Cell Transcriptomics for Plant Research. Annual Review of Plant Biology **72**: 847-866.

60. Shahan, R., Hsu, C.W., Nolan, T.M., Cole, B.J., Taylor, I.W., Greenstreet, L., Zhang, S., Afanassiev, A., Vlot, A.H.C., Schiebinger, G., Benfey, P.N. and Ohler, U. (2022). A single-cell *Arabidopsis* root atlas reveals developmental trajectories in wild-type and cell identity mutants. Developmental Cell **57**: 543-560.e9.

61. Shao, X., Liao, J., Lu, X., Xue, R., Ai, N. and Fan, X. (2020). scCATCH: Automatic Annotation on Cell Types of Clusters from Single-Cell RNA Sequencing Data. iScience **23**: 100882.

62. Shulse, C.N., Cole, B.J., Ciobanu, D., Lin, J., Yoshinaga, Y., Gouran, M., Turco, G.M., Zhu, Y., O'Malley, R.C., Brady, S.M. and Dickel, D.E. (2019). High-Throughput Single-Cell Transcriptome Profiling of Plant Cell Types. Cell Reports **27**: 2241-2247.e4.

63. Stuart, T., Butler, A., Hoffman, P., Hafemeister, C., Papalexi, E., Mauck, W.M., Hao, Y., Stoeckius, M., Smibert, P. and Satija, R. (2019). Comprehensive Integration of Single-Cell Data. Cell **177**: 1888-1902.e21.

64. Tandon, D., De Farias, T.M., Allard, P.-M. and Defossez, E. (2026). METRIN-KG: A knowledge graph integrating plant metabolites, traits, and biotic interactions. GigaScience **15**: giag051.

65. Tarashansky, A.J., Musser, J.M., Khariton, M., Li, P., Arendt, D., Quake, S.R. and Wang, B. (2021). Mapping single-cell atlases throughout Metazoa unravels cell type evolution. eLife **10**: e66747.

66. Tenorio Berrío, R. and Dubois, M. (2024). Single-cell transcriptomics reveals heterogeneity in plant responses to the environment: a focus on biotic and abiotic interactions. Journal of Experimental Botany **75**: 5188-5203.

67. The Gene Ontology Consortium (2023). The Gene Ontology knowledgebase in 2023. Genetics **224**: iyad031.

68. Theodoris, C.V., Xiao, L., Chopra, A., Chaffin, M.D., Al Sayed, Z.R., Hill, M.C., Mantineo, H., Brydon, E.M., Zeng, Z., Liu, X.S. and Ellinor, P.T. (2023). Transfer learning enables predictions in network biology. Nature **618**: 616-624.

69. Traag, V.A., Waltman, L. and van Eck, N.J. (2019). From Louvain to Leiden: guaranteeing well-connected communities. Scientific Reports **9**: 5233.

70. Tung, C.-C., Kuo, S.-C., Yang, C.-L., Yu, J.-H., Huang, C.-E., Liou, P.-C., Sun, Y.-H., Shuai, P., Su, J.-C., Ku, C. and Lin, Y.-C.J. (2023). Single-cell transcriptomics unveils xylem cell development and evolution. Genome Biology **24**: 3.

71. Walls, R.L., Athreya, B., Cooper, L., Elser, J., Gandolfo, M.A., Jaiswal, P., Mungall, C.J., Preece, J., Rensing, S., Smith, B. and Stevenson, D.W. (2012). Ontologies as integrative tools for plant science. American Journal of Botany **99**: 1263-1275.

72. Wang, Y., Huan, Q., Li, K. and Qian, W. (2021). Single-cell transcriptome atlas of the leaf and root of rice seedlings. Journal of Genetics and Genomics **48**: 881-898.

73. Wolf, F.A., Angerer, P. and Theis, F.J. (2018). SCANPY: large-scale single-cell gene expression data analysis. Genome Biology **19**: 15.

74. Xu, X., Crow, M., Rice, B.R., Li, F., Harris, B., Liu, L., Demesa-Arevalo, E., Lu, Z., Wang, L., Fox, N., Wang, X., Drenkow, J., Luo, A., Char, S.N., Yang, B., Sylvester, A.W., Gingeras, T.R., Schmitz, R.J., Ware, D., Lipka, A.E., Gillis, J. and Jackson, D. (2021). Single-cell RNA sequencing of developing maize ears facilitates functional analysis and trait candidate gene discovery. Developmental Cell **56**: 557-568.e6.

75. Xue, H.-C., Xu, Z.-G., Liu, Y.-J., Wang, L., Ming, X., Wu, Z.-Y., Lian, H., Han, Y.-W., Xu, J., Zhang, Z.-D., Shao, Q.-L., Liu, K., Wang, F.-X., Wang, A.-H., Zhao, J., Zhang, J., Zhang, J., Chen, J., Mao, Y. and Wang, J.-W. (2025). A unified cell atlas of vascular plants reveals cell-type foundational genes and accelerates gene discovery. Cell **188**: 6370-6390.e29.

76. Yang, Z., Wu, Y., Li, Y., Ling, H.-Q. and Chu, C. (2009). OsMT1a, a type 1 metallothionein, plays the pivotal role in zinc homeostasis and drought tolerance in rice. Plant Molecular Biology **70**: 219-229.

77. Yin, R., Xia, K. and Xu, X. (2023). Spatial transcriptomics drives a new era in plant research. The Plant Journal **116**: 1571-1581.

78. Yu, X., Liu, Z. and Sun, X. (2023). Single-cell and spatial multi-omics in the plant sciences: Technical advances, applications, and perspectives. Plant Communications **4**: 100508.

79. Zhang, A.W., O'Flanagan, C., Chavez, E.A., Lim, J.L.P., Ceglia, N., McPherson, A., Wiens, M., Walters, P., Chan, T.H.M., Hewitson, B., Lai, D., Mottok, A., Sarkozy, C., Chong, L.C., Aoki, T., Wang, X., Weng, A.P., McAlpine, J.N., Aparicio, S., Steidl, C., Campbell, K.R. and

Shah, S.P. (2019). Probabilistic cell-type assignment of single-cell RNA-seq for tumor microenvironment profiling. Nature Methods **16**: 1007-1015.

80. Zhang, J., Chen, X., Song, Y. and Gong, Z. (2024). Integrative regulatory mechanisms of stomatal movements under changing climate. Journal of Integrative Plant Biology **66**: 368-393.

81. Zheng, D., Lu, X., Lu, Y., Liang, P., Shang, N., Xu, J., Yao, J., Mo, F., Chu, Q., Fan, L. and Chen, H. (2026). PlantscRNAdb 4.0: Improved marker identification and annotation under a cell-type uniformity for plants. Molecular Plant **19**: 673-688.

82. Zhong, H., Han, W., Gomez-Cabrero, D., Tegner, J., Gao, X., Cui, G. and Aranda, M. (2025). Benchmarking cross-species single-cell RNA-seq data integration methods: towards a cell type tree of life. Nucleic Acids Research **53**: gkae1316.

Supplementary Information

Supplementary Figure S1. Conceptual workflow showing how Xener resolves hidden intracluster heterogeneity.

Supplementary Figure S2. Assessment of species-level consistency across datasets and analytical results.

Supplementary Figure S3. Application of the analysis workflow to the Catharanthus roseus SRP335448 dataset.

Supplementary Figure S4. Comparative evaluation of Xener and Xener-Skill across 62 datasets.

Supplementary Figure S5. Classification of orthogroups according to their levels of evolutionary conservation.

Supplementary Figure S6. Web-based interactive exploration and subcluster refinement of the analysis results.

Supplementary Data Set 1. Species-level composition and evidence coverage of the Xener knowledge graph marker resource.

Supplementary Data Set 2. Standardized PO terms, harmonized cell-type nomenclature and marker evidence coverage.

Supplementary Data Set 3. Cell type-level conservation of marker evidence and orthogroup associations across species.

Supplementary Data Set 4. Benchmark dataset resources, species, tissues and accession information used for cross-species annotation.

Supplementary Data Set 5. Sensitivity of cross-species annotation to cumulative reference-species composition for *A. thaliana* and *S. bicolor*.

Supplementary Data Set 6. Comparative annotation performance and cell-type composition across methods in CRA006988.

Supplementary Data Set 7. Transcriptional support and independent reference validation for Xener refinement of the original Bundle sheath population in CRA006988.

Supplementary Data Set 8. Complete *B. rapa* query-gene to *A. thaliana* homolog evidence mapping underlying the traceable cell-type annotation network.

Supplementary Data Set 9. Species- and cell type-specific distributions of Core, Broad, Narrow and Unique marker occurrences.

Supplementary Data Set 10. Motif groups and functional annotations of Core phloem marker records.

Supplementary Data Set 11. Cluster-level expression profiles and expression specificity of representative Core phloem markers.

Supplementary Data Set 12. Cell-level comparison of Xener-Refine assignments with expression-only Leiden reclustering.

Supplementary Data Set 13. Gene Ontology enrichment of graph-derived genes supporting the Xener-Refine cell-type assignments.

Supplementary Data Set 14. Candidate cell-type support underlying bamboo spatial annotation and refinement shown in Figure 6b.

Supplementary Data Set 15. Quantitative support for bamboo spatial cluster refinement and subgroup assignments.

Supplementary Data Set 16. Pairwise refinement comparisons and global annotation support for Moso bamboo spatial clusters, with selected Figure 6c gene evidence.

Supplementary Data Set 17. Organ-matched *A. thaliana* reference datasets and processed accession identifiers used for the SATURN analyses.

Supplementary Files

This is a list of supplementary files associated with this preprint. Click to download.

- SupplementaryDataSet.xlsx
- SupplementaryFigureS1S6.pdf